Lawrence Berkeley National Laboratory

Title

Dimorphic Mechanisms of Fragility in Diabetes Mellitus: the Role of Reduced Collagen Fibril Deformation

Permalink

https://escholarship.org/uc/item/8z24g29g

Journal

Journal of Bone and Mineral Research, 37(11)

ISSN

0884-0431

Authors

Wölfel, Eva M
Schmidt, Felix N
Scheidt, Annika vom
et al.

Publication Date

2020-12-01

DOI

10.1002/jbmr.4706

Copyright Information

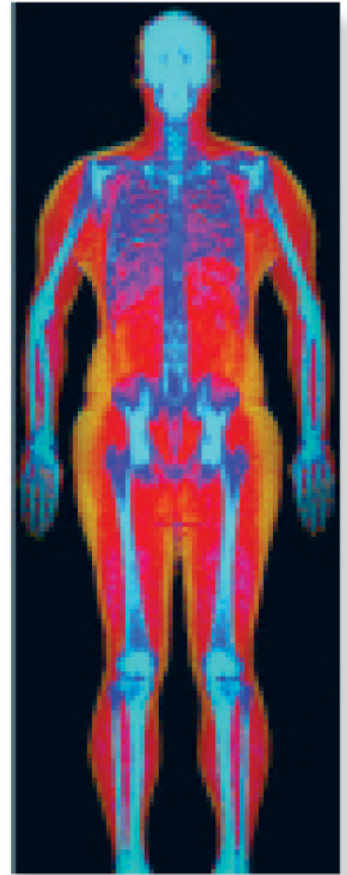Peer reviewed

HOLOGIC®
The Science of Sure

Powerful images.
Clear answers.

Manage Patient's concerns about Atypical Femur Fracture*

Vertebral Fracture Assessment – a critical part of a complete fracture risk assessment

Advanced Body Composition® Assessment – the power to see what's inside

Contact your Hologic rep today at BSHSalesSupportUS@hologic.com

Dimorphic Mechanisms of Fragility in Diabetes Mellitus: the Role of Reduced Collagen Fibril Deformation

Eva M. Wölfel,[1,2] Felix N. Schmidt,[1] Annika vom Scheidt,[1,3] Anna K. Siebels,[1] Birgit Wulff,[4] Herbert Mushumba,[4] Benjamin Ondruschka,[4] Klaus Püschel,[4] Jean Scheijen,[5] Casper G. Schalkwijk,[5] Eik Vettorazzi,[6] Katharina Jähn-Rickert,[1,7] Bernd Gludovatz,[8] Eric Schaible,[9] Michael Amling,[1] Martina Rauner,[10,11,12] Lorenz C. Hofbauer,[10,11,12] Elizabeth A. Zimmermann,[13] and Björn Busse[1,2]

[1]Department of Osteology and Biomechanics, University Medical Center Hamburg-Eppendorf, Hamburg, Germany
[2]Interdisciplinary Competence Center for Interface Research (ICCIR), University Medical Center Hamburg-Eppendorf, Hamburg, Germany
[3]Department of Macroscopic and Clinical Anatomy, Gottfried Schatz Research Center, Medical University of Graz, Graz, Austria
[4]Institute of Legal Medicine, University Medical Center Hamburg-Eppendorf, Hamburg, Germany
[5]Department of Internal Medicine, Cardiovascular Research Institute Maastricht (CARIM) School for Cardiovascular Diseases, Maastricht University, Maastricht, The Netherlands
[6]Institute of Medical Biometry and Epidemiology, University Medical Center Hamburg-Eppendorf, Hamburg, Germany
[7]Mildred Scheel Cancer Career Center Hamburg, University Cancer Center Hamburg, University Medical Center Hamburg-Eppendorf, Hamburg, Germany
[8]School of Mechanical and Manufacturing Engineering, University of New South Wales (UNSW Sydney), Sydney, New South Wales, Australia
[9]Advanced Light Source, Lawrence Berkeley National Laboratory, Berkeley, CA, USA
[10]Department of Medicine III, Technische Universität Dresden Medical Center, Dresden, Germany
[11]Center for Healthy Aging, Technische Universität Dresden Medical Center, Dresden, Germany
[12]Center for Regenerative Therapies Dresden, Technische Universität Dresden, Dresden, Germany
[13]Faculty of Dental Medicine and Oral Health Sciences, McGill University, Montreal, Quebec, Canada

ABSTRACT

Diabetes mellitus (DM) is an emerging metabolic disease, and the management of diabetic bone disease poses a serious challenge worldwide. Understanding the underlying mechanisms leading to high fracture risk in DM is hence of particular interest and urgently needed to allow for diagnosis and treatment optimization. In a case–control postmortem study, the whole 12th thoracic vertebra and cortical bone from the mid-diaphysis of the femur from male individuals with type 1 diabetes mellitus (T1DM) ($n = 6$; 61.3 ± 14.6 years), type 2 diabetes mellitus (T2DM) ($n = 11$; 74.3 ± 7.9 years), and nondiabetic controls ($n = 18$; 69.3 ± 11.5) were analyzed with clinical and ex situ imaging techniques to explore various bone quality indices. Cortical collagen fibril deformation was measured in a synchrotron setup to assess changes at the nanoscale during tensile testing until failure. In addition, matrix composition was analyzed including determination of cross-linking and non-crosslinking advanced glycation end-products like pentosidine and carboxymethyl-lysine. In T1DM, lower fibril deformation was accompanied by lower mineralization and more mature crystalline apatite. In T2DM, lower fibril deformation concurred with a lower elastic modulus and tendency to higher accumulation of non-crosslinking advanced glycation end-products. The observed lower collagen fibril deformation in diabetic bone may be linked to altered patterns mineral characteristics in T1DM and higher advanced glycation end-product accumulation in T2DM. © 2022 The Authors. *Journal of Bone and Mineral Research* published by Wiley Periodicals LLC on behalf of American Society for Bone and Mineral Research (ASBMR).

KEY WORDS: advanced glycation end-products; bone quality; collagen deformation; cortical bone; diabetes mellitus

Introduction

Diabetes mellitus (DM) is a severe chronic condition occurring in about 19.3% of adults over 65 years old.[1,2] DM can result in long-term organ damage leading to life-threatening health complications by promoting cardiovascular diseases, nerve damage (neuropathy), kidney damage (nephropathy), eye disease (retinopathy, visual loss, blindness), and musculoskeletal problems. There are two main types of DM: type 1 diabetes mellitus (T1DM), occurring in children or young adults, is an autoimmune disease, leading to absolute insulin deficiency, and type 2 diabetes mellitus (T2DM), usually occurring in older individuals is an inflammatory disease leading to insulin resistance. Both types eventually manifest in hyperglycemia and may cause microvascular and macrovascular complications. Approximately 90% of all DM cases are T2DM. Bone, as an endocrine organ, has also been shown to be affected by DM.[3] Specifically, DM is associated with increased nonvertebral bone fracture risk,[4,5] impaired bone fracture healing,[6] and higher postfracture mortality.[7] However, the exact cause and mechanisms of these skeletal complications are still unknown.

Individuals with T1DM have normal to low bone mineral density (BMD). Commonly, fracture risk is determined based on areal BMD values obtained with dual-energy X-ray absorptiometry (DXA). In comparison to healthy young controls a sevenfold higher hip fracture risk was reported in T1DM patients.[8] Individuals with T2DM have normal or high BMD and a relative risk of hip fracture of 1.2 compared to nondiabetic patients.[9] Thus, in DM, BMD fails to fully explain fracture risk[10,11] and is not sufficient to identify those at risk of fracture. Additional microarchitectural information obtained with high-resolution peripheral quantitative computed-tomography (HR-pQCT) only indicate differences when analyzing subgroups such as T2DM with previous fractures[12] or T1DM with microvascular disease.[13] However, although these subgroups may be identified beforehand based on clinical records, the reason for the increased fracture risk largely remains unknown. Furthermore, focusing on these subgroups excludes patients without fractures or microvascular diseases, who might be at increased fracture risk.

Although in general fracture risk is associated with bone loss, diabetic patients experience a higher fracture risk for a similar T-score than nondiabetic individuals despite a similar T-score.[14] This suggests that diabetes-related changes may influence bone material properties constituting bone quality and thereby contributing to greater fracture risk.[15] Bone quality is a combination of different inherent bone characteristics, such as bone geometry and microstructure, bone remodeling status, as well as collagen and mineral properties. At the smallest size scale, bone consists of mineral nanoplatelets embedded within a collagen matrix. The mineral provides stiffness and reinforcement, whereas the collagen phase contributes ductility for energy absorption. Collagen deformation plays a major role in bone-toughening mechanisms because collagen fibrils are able to absorb tissue strain by elastic stretching and inelastic mechanisms, such as sliding of collagen fibrils.[16,17] This mechanism at the nanoscale can prevent strain-induced cracking at higher length-scales, which would otherwise lead to fracture and failure of the bone. Posttranslational modifications of the collagen fibrils in the form of enzymatic cross-links or advanced glycation end-products (AGEs), with the latter being formed through glycation of the bone matrix proteins via nonenzymatic reactions with sugar molecules, further stiffen the collagenous bone matrix affecting the collagen properties and its responses to mechanical loading or forces.[16] Therefore, accessing collagen deformation is of high importance when aiming to determine factors contributing to reduced bone toughness. High urinary pentosidine, a fluorescent and cross-linking AGE, has been identified as a risk factor for fractures in T2DM,[18] and investigations of bone matrix properties in T1DM and T2DM indicate changes in nonenzymatic cross-linking profile and mineralization.[19-21] Specifically, higher pentosidine content was found in the trabecular part of iliac crest biopsies from fracturing patients with T1DM compared to healthy controls.[21] In T2DM, higher pentosidine content was described in trabecular bone tissue from individuals undergoing total hip arthroplasty,[19] whereas fluorescent AGEs in cortical and trabecular bones tissue were observed to be similar between T2DM and control groups.[19,20,22] More recently, accumulation of the non-cross-linking AGE N$^\varepsilon$-carboxymethyl-lysine (CML) has been described to be more abundant in cortical bone[23] than pentosidine and to be higher in cortical bone of T2DM individuals independent of cortical porosity compared to healthy individuals.[20] Circulating CML levels are associated with higher fracture risk in T2DM patients independent of BMD.[24] CML may form through methylglyoxal, which has been shown to be higher in patients with DM.[25] Other AGEs that are derived from methylglyoxal are N$^\varepsilon$-carboxyethyl-lysine and N$^\delta$-(5-hydro-5-methyl-4-imidazolon-2-yl)-ornithine 1 (MG-H1), the latter together with CML were higher in serum and bone tissue of a non-obese T2DM mouse model.[26]

Fracture resistance of bone is also determined by the cortical bone microarchitecture, with cortical bone seen as major contributor to bone strength in the femoral neck.[27] Features of the cortical microstructure, such as osteons and cement lines, resist crack propagation and thereby influence fracture resistance. Osteons are the basic structural units of cortical bone produced during bone remodeling. Low bone turnover evident by biochemical serum markers and histomorphometry indices are characteristic findings in DM,[10,11,20,28-30] which could impact fracture resistance by altering bone matrix composition, normal cycles of damage repair, and the density and size of osteons at the microstructural level. For example, impaired indentation properties in cortical bone[22] and higher sugar content bound to the collagen matrix along with higher mineral content[19] have been shown in patients with T2DM and osteoarthritis undergoing total hip arthroplasty. Higher degree of mineralization and higher nonenzymatic cross-linking were found in T1DM with previous fractures in trabecular bone.[21]

Previous studies have shown that AGEs induced in vitro and due to aging in vivo resulted in lower collagen fibril deformation and collagen stiffening,[16,31] whereas studies assessing collagen deformation in diabetic bone tissue are scarce. Here, we hypothesize that in individuals with DM AGEs accumulate in the bone matrix affecting the deformation properties of collagen fibrils. We investigate the underlying mechanisms of higher fracture risk in DM by focusing on clinical fracture risk assessment via bone density and microarchitecture measures in combination with experimentally determined material properties emphasized by bone matrix composition and mechanical behavior under load. The initial aim of our study was to determine whether DM collagen deformation differs from age- and body mass index (BMI)-matched healthy controls. We apply a top-down approach by first analyzing all DM cases together followed by differentiation into T1DM and T2DM cases to allow for identification of type-specific mechanisms. Although in previous studies a

high cortical porosity subgroup within the T2DM group was identified,[12,32] here we focus on cases with similar cortical porosity to the control group measured with HR-pQCT to assess differences in bone quality independent of cortical porosity. Our previous study[20] demonstrated higher accumulation of the non-crosslinking AGE CML and altered mineralization degree between the T2DM and control groups independent of cortical porosity. We hypothesize that collagen fibril deformation is lower in DM cases and that it results from different bone matrix changes due to the distinct pathophysiology of T1DM and T2DM.

Materials and Methods

Study design

In this study, we aim to determine effects of DM and specifically distinct effects of T1DM and T2DM, on the cortical bone matrix at the fibril nanoscale in combination with bone matrix composition and clinical high-resolution imaging (Fig. 1). Therefore, we obtained femoral bone of the mid-diaphysis of approximately 2 cm in length and the 12th thoracic and adjacent vertebrae

postmortem from male organ donors during autopsy in collaboration with the Institute of Legal Medicine at the University Medical Center Hamburg-Eppendorf as approved by the local institutional ethics review board (WT037/15). For the case–control study a total number of 35 samples were collected of which 17 individuals (mean ± standard deviation [SD], age 69.7 ± 12.1 years) were known to be diagnosed with DM based on medical history reports (six individuals were diagnosed with T1DM and 11 individuals with T2DM). Additionally, 18 age- and BMI-matched healthy individuals (mean ± SD, age 69.3 ± 11.3 years) were collected as control group. The sample size for this study was determined in line with the primary focus on the assessment of collagen fibril deformation characteristics in individuals with DM and age-matched healthy controls. Therefore, the power analysis was based on a previous study, where collagen fibril deformation was measured in young and aged human cortical bone ($n = 7$ and $n = 6$, respectively).[16] A similar effect size was expected due to the outcome of the former study showing significantly lower fibril strain in bone tissue from aged individuals compared to young individuals. Deidentified data (age, height, weight, diabetes status, and medication) were
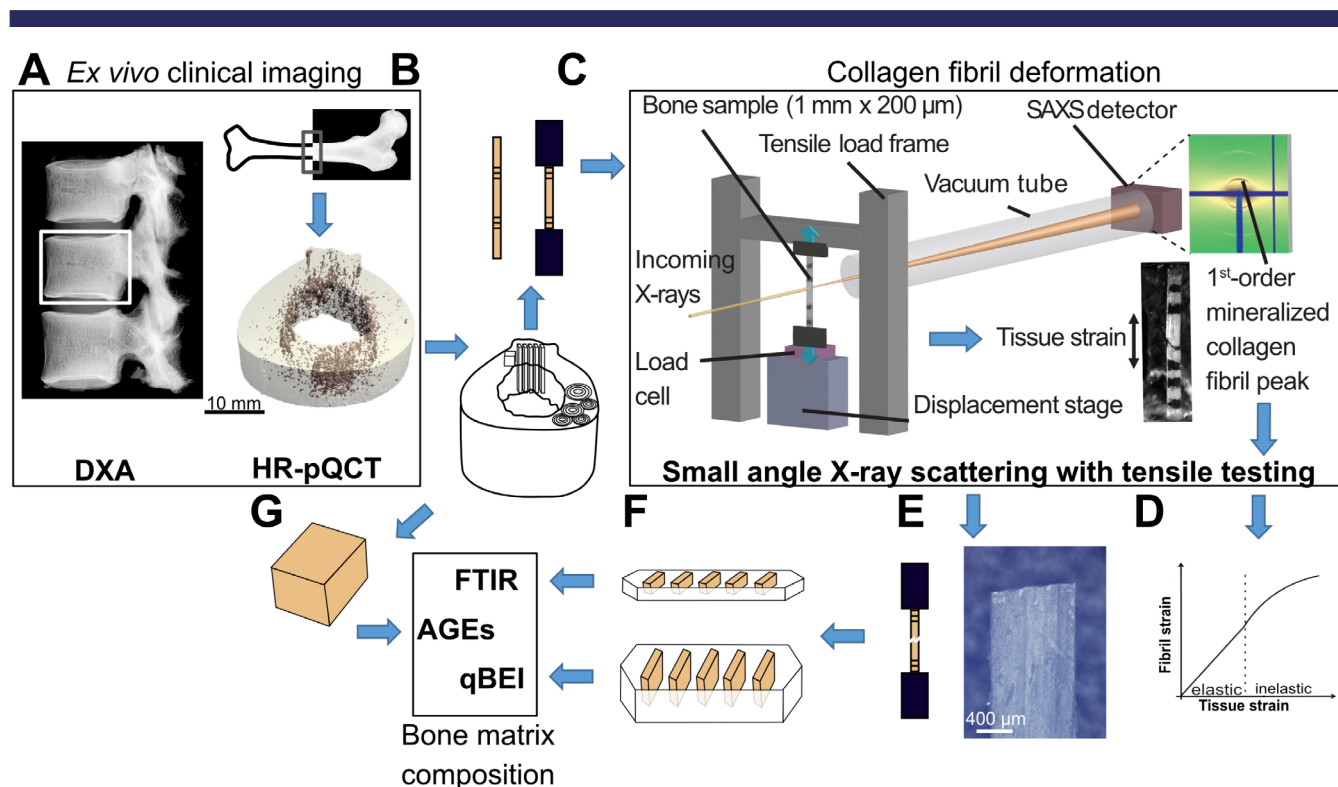
Fig. 1. Workflow of the experimental setup. (A) Ex vivo clinical imaging of the 12th thoracic vertebra using dual energy X-ray absorptiometry and of the mid-diaphysis of the femur using high-resolution peripheral quantitative computed tomography. (B) Small bone samples were prepared from the posterior quadrant of the femoral cross-section in longitudinal osteon direction, marked, and grid paper was glued to the ends. (C) Schematic of synchrotron setup for small angle X-ray scattering with simultaneous tensile testing of small-scale human cortical bone samples. During tensile testing, the periodicity of the mineralized collagen fibril diffracts X-ray at small angles. The d-period of the collagen fibril, measured from the diffraction pattern, changes position during tensile testing indicating deformation of the fibril. Based on macroscopic images of the bone sample during tensile testing, the tissue strain was calculated. (D) Analysis of the data allowed plotting the fibril strain versus tissue strain and division of elastic and inelastic regions. (E) Bone samples following tensile testing until failure. (F) Embedded fracture surfaces of bone samples following tensile testing for backscattered electron microscopy and sectioning of 2-μm-thick bone sections for Fourier transform infrared spectroscopy analysis. (G) Bone cube extracted from the frozen mid-diaphyseal femoral bone tissue in vicinity to the extracted bone samples for tensile testing for advanced glycation end-product analysis. AGE = advanced glycation end-product; DXA = dual-energy X-ray absorptiometry; FTIR = Fourier transform infrared spectroscopy; HR-pQCT = high-resolution peripheral quantitative computed tomography; qBEI = quantitative backscattered electron microscopy.

acquired for each individual. Exclusion criteria were any bone diseases; eg, osteogenesis imperfecta, fibrous dysplasia, malignancy, Paget's disease of bone, etc. Additionllally, individuals with renal or hepatic disorders, hyperparathyroidism, and bedrest were excluded. In the diabetic cases, antidiabetic treatments for T2DM ranged from oral antidiabetics (six individuals) such as metformin to insulin treatment (three individuals), whereas individuals with T1DM were all treated with insulin. Both, the 12th thoracic vertebra, which is used to determine BMD via ex vivo DXA measurement, and the femoral cross-section cleaned of soft tissue were wrapped in gauze soaked with phosphate buffered saline (PBS) and stored at $-20°C$ prior to further processing. All analysis were performed blinded.

DXA

Using an ex vivo protocol, DXA (GE Healthcare, Berlin, Germany) was applied to the 12th thoracic vertebra (Fig. 1A) to determine the BMD of each donor, which is generally used to calculate the *T*-score according to the World Health Organization, to assure no individual had undiagnosed osteoporosis. To compensate for missing soft tissue a water phantom producing a water column of 15 cm was utilized, which was provided by the manufacturer for DXA calibration and simulates the thickness of soft tissue of a person with body weight of 70 kg and height of 170 cm. The vertebrae were positioned in a plastic container filled with water and the water phantom was placed on top as reported.[33] With the software provided by the manufacturer, BMD values from anterior–posterior (AP) and lateral (LAT) scan directions were obtained. Due to destruction of single vertebrae during extraction a total number of 16 controls and 14 diabetes mellitus cases were scanned and evaluated.

HR-pQCT

Frozen femoral cross-sections were scanned with HR-pQCT (Xtreme CT I; Scanco Medical AG, Brüttisellen, Switzerland; Fig. 1A) to compare clinically assessments of the bone tissue to bone material quality analyses. Weekly and daily calibration was performed for quality assurance with phantoms provided by the manufacturer. For each sample analyzed (14 controls and 14 diabetes mellitus cases) a minimum of 110 slices (based on common clinical HR-pQCT scans) were scanned with a resolution of 82-μm voxels with 750 projections over 180 degrees and an integration time of 100 ms at each angular position. For the scan, frozen femoral samples were placed into an ex vivo sample holder provided by the manufacturer and the central region of the extracted femoral mid-diaphysis was chosen as region of interest to avoid inclusion of regions with extraction artifacts. Following reconstruction, images were analyzed with the software provided by the manufacturer according to previously published protocols by Burghardt and colleagues[34] where a fixed global threshold was applied (40% of the maximum possible grayscale value). In detail, the peripheral cortical bone structure was contoured, followed by analysis with the standard evaluation routine provided by the manufacturer. Then, the endocortical contour (automatically drawn with the standard evaluation routine) is inspected visually. If required, the endocortical contour is manually corrected and the standard evaluation routine is re-run. The final evaluation program calculated the following cortical parameters; cortical area (Ct.Ar, mm²), cortical volumetric bone mineral density (Ct.vBMD, mg hydroxyapatite [HA]/cm³), cortical thickness (Ct.

Th, mm), cortical perimeter (Ct.Pm, mm), cortical porosity (Ct. Po, %), and cortical pore diameter (Ct.Po.Dm, μm).[34]

Small angle X-ray scattering with simultaneous tensile testing

Testing setup

The mechanical properties at the fibrillar length scale were analyzed via synchrotron small-angle X-ray scattering (SAXS) experiments with simultaneous tensile testing as reported.[35] By this, it was aimed to determine whether collagen fibril deformation is reduced in diabetic bone compared to age-matched healthy bone. Cortical bone samples (17 controls and 18 diabetes mellitus cases) were cut to dimensions of 20 mm × 1 mm × 250 μm with a band saw and fixed in 70% ethanol for 7 seconds, and then air-dried to allow silicon carbide paper attachment. Silicon carbide paper was glued to the ends of the sample with cyanoacrylate glue to provide a surface grip during tensile testing (Fig. 1B). Five samples of cortical bone per each individual sample were prepared and rehydrated in Hanks' Balanced Salt Solution (HBSS) for 6 hours prior to testing. Fixation with ethanol dehydrates bone tissue which may strengthen the collagen fibrils and embrittle the collagen phase[36]; however, it was required for secure testing of biological material in the synchrotron. All samples underwent the same procedure including rehydration of the bone samples, which have been shown to restore biomechanical properties following ethanol dehydration.[37] During the experiment, a tensile test was performed on the bone while it was simultaneously exposed to X-rays[16] (Fig. 1C). The strain in the collagen fibrils was measured as the X-rays were scattered in dependence of the regular periodicity of the mineralized collagen fibril, causing an intensity peak that shifted position during the tensile test, as the periodicity increased.[35]

Data collection

Data collection included measurements of the load, images of the samples surface for tissue strain determination, and two-dimensional (2D) small angle X-ray scattering patterns for fibril strain measurement (Fig. 1C). Therefore, the samples were loaded in a Linkam TST-350 tensile stage (Linkam Scientific Instruments Ltd., Tadworth, UK), which was positioned in beamline 7.3.3 at the Advanced Light Source (ALS)[38] synchrotron radiation facility (Lawrence Berkeley National Laboratory, Berkeley, CA, USA) with a 10-mm distance between the grips and a displacement rate of 1 μm/s until failure. To collect the SAXS data a high-speed Pilatus3 2 M detector (Dectris, Baden, Switzerland) was positioned approximately 4000 mm from the sample using an X-ray energy of 10 keV. Data was collected for 0.5 second at 10-second intervals. Calibration of the sample-to-detector distance and localization of the beam center was performed from X-ray exposure of a silver behenate standard sample was performed using the analysis software Igor Pro (Wavemetricx, Portland, OR, USA) in conjunction with the custom macro NIKA.[39]

Data analysis

After calibration, custom software written in LabVIEW (National Instruments, Austin, TX, USA) was used to analyze the data. For each image, the image was first remapped from Cartesian to polar coordinates, and then background scattering was subtracted from the remapped images using weighted spline functions. The first order peak from the collagen appears as an arc

in the SAXS images (Fig. 1C), and the angular center of this arc was identified by fitting the azimuthal intensity with a Gaussian function. An azimuthal integration was then performed, using a ± 5-degree wedge running through the center of the arc, which summed the intensity values at each radial distance starting at the beam center and traveling radially outward. This gave a profile describing the changes in intensity with respect to q value (radial distance from beam center) and enabled the location of the collagen peak in q-space to be found by fitting the peak with an exponentially modified Gaussian function. The resulting q-space value for peak location was then converted into a real space length using length $= 2\pi/(q\text{-location})$. This value measured the center of the distribution of d-periods (lengths of repeated subunits) present in the collagen fibrils. Using this value, we could then calculate what the collagen fibril d-period size was determined at each point during the tensile test (Fig. 1C) and fibril strain was calculated, by using the change in d-period length divided by the length at zero load. Overall tissue strain was measured separately, using charge-coupled device (CCD) images of the bone, which had multiple lines marked upon its surfaces (Fig. 1C). The separation between the lines were measured using National Instruments Vision Assistant 8.5 (National Instruments, Austin, TX, USA), and the tissue strain was measured as the change in line separation divided by the separation at zero load. Load and strain data were acquired simultaneously with X-ray exposure every 10 seconds. Therefore, the full stress–strain curves were not recorded including the point of material failure.

Function of fibril strain to tissue strain ratio

After data processing, fibril strain as a function of tissue strain can be determined (Fig. 1D). The elastic fibril strain over tissue strain was determined based on the slopes of linear regressions of each tested bone sample in the elastic range of the fibril-tissue strain graph (<0.55% tissue strain). Following the elastic/inelastic transition, the inelastic range was defined above 0.55% tissue strain. The elastic modulus was based on the slopes of the linear regressions of the tissue stress–strain diagram in the elastic range (<0.55% tissue strain). Data were collected every 10 seconds; therefore, the full stress–strain curve for the test sample was not recorded. For this reason, the limit of 0.55% was chosen because all curves below this limit have a linear relationship between stress and strain.

Quantitative backscattered electron microscopy

Following mechanical testing, samples used for SAXS were embedded in methylmethacrylate (MMA; Fig. 1E) to allow for analysis of the samples' fracture surfaces (18 control and 12 DM cases). Subsequent analysis of the mechanically tested bone tissue tested was performed to further determine mineral and matrix properties of the diabetic and control bone tissue and link these to the collagen fibril deformation results. Per each diabetes or control case, all tensile tested bone samples were embedded in one block so that the fracture side was available for subsequent analysis (Fig. 1F). Evaluation of bone mineral density distribution (BMDD) was performed via quantitative backscattered electron microscopy (qBEI) on the coplanar and polished MMA blocks with exposed fracture side of the tested bone samples. Prior to imaging the samples were carbon coated. The scanning electron microscope (Crossbeam 340; Carl Zeiss AG, Oberkochen, Germany) was operated in backscattered electron mode (BSD4-Detector; Zeiss) with 20 keV, a working

distance of 20 mm, and a constant beam current. The beam current was controlled by a Faraday cup (MAC Consultant Ltd., Knowlhill, UK) and grayscale values were calibrated on an aluminum-carbon standard. According to Roschger and colleagues,[40] the standard material was used to convert grayscale values to Ca wt%, which takes advantage of the known atomic numbers ($Z = 6$ for carbon and $Z = 13$ for aluminum). By using the same brightness and contrast of the backscattered electron detector amplifier, the grayscale values were adjusted to obtain 222.4 ± 0.5 for aluminum and 5.0 ± 0.5 for carbon. On the Z-grayscale value diagram the measured points of the reference material were connected through a straight line which serves as correlation of grayscale values and atomic numbers. All parameters were maintained constant during imaging and BMDD was determined based on grayscale values according to established protocols.[41] One to two images per sample with magnification $\times 200$ were acquired to image the entire region of each sample. The parameters mean calcium weight percentage (Ca Mean, wt%), most frequent calcium weight percentage (Ca Peak, wt%), SD of the calcium content curve displaying the heterogeneity of BMDD (Ca Width, wt%), percentage of bone area mineralized below the fifth percentile of the reference range of the control group (Ca low, % bone area), and percentage of bone area containing calcium concentration above the 95th percentile of the control group (Ca high, % bone area) were determined. The parameters were assessed using a customized Matlab routine (MATLAB R2014a; MathWorks, Natick, MA, USA).

Fourier transform infrared spectroscopy

To allow for analysis of the matrix composition, Fourier transform infrared spectroscopy (FTIR) was performed (18 control and 12 DM cases). The blocks of embedded bone (following SAXS) were cut with a microtome to produce a bone section with a maximum thickness of 2 μm (Fig. 1F) and transferred to a plate with holes to allow for transmission of infrared light. During embedding, the region of fracture was facing the cutting plane and the first full bone section after the fracture surface was used for further analysis. Using a Spotlight 400 system (PerkinElmer, Waltham, MA, USA) attached to the Frontier 400 spectrometer, measurements on each sample were performed over a bone area of 150 μm × 150 μm. The measured area was chosen to contain as much bone tissue as possible aiming to minimize inclusion of voids. Sixteen scans per pixel were acquired with a wavenumber range from 4000 to 570 cm^{-1} and a resolution of 2 cm^{-1} wavenumbers. FTIR measurements were post processed by subtraction of Poly(methyl methacrylate) (PMMA) signal and smoothing of absorbance signal. Additionally, linear baseline removal was performed prior to spectral analysis with a custom written Matlab script.[42] Main peaks were located as the phosphate peak between 1154 and 900 cm^{-1}, the carbonate peak between 890 and 850 cm^{-1}, and the amide I peak between 1710 and 1600 cm^{-1}. Assessed bone tissue parameters included carbonate-to-phosphate ratio (area of carbonate/phosphate) and mineral-to-matrix ratio (area of phosphate/amide I). Based on the second derivative of the original spectra and established peak positions,[42,43] subpeaks of interest of amide I and phosphate peak were identified. After subpeak fitting for the phosphate peak the mineral crystallinity (phosphate subpeaks 1020/1030 cm^{-1}) and mineral maturity (phosphate subpeaks 1030/1108 cm^{-1}) were assessed. Furthermore, based on the previously described individual peaks 1109 and 996 cm^{-1},[44] the ratio of poorly crystalline apatites over

PO_4^{-3} in apatitic environment (phosphate sub-peaks 1109/996 cm^{-1}) was determined. Based on the amide I subpeak-fitting, a number of parameters including matrix maturity (amide I subpeaks 1660/1692 cm^{-1}), enzymatic cross-linking ratio (amide I subpeaks 1660/1678 cm^{-1}), and nonenzymatic cross-linking ratio (amide I subpeaks 1678/1692 cm^{-1}) were determined.[42]

Fluorescent AGEs

To determine whether different AGE accumulations are observed in the diabetic bone compared to healthy bone, total fluorescent AGEs (fAGEs) were quantified using fluorescence spectroscopy and normalized to collagen content assessed by colorimetric assay[20] to determine whether different AGE accumulation is observed in diabetic bone compared to healthy bone. Small bone samples from frozen femoral bone (Fig. 1G) adjacent to the extraction side of the samples prepared for tensile testing (18 controls and 16 DM cases) were defatted by alternate soaking for 15 minutes in either 70% ethanol and saline. After lyophilization for 18 hours, the bone samples were hydrolyzed in 6 N HCl at 110°C for 16 hours. Bone hydrolysates were diluted in deionized water to a final concentration of 0.5 mg bone/mL. To determine the total collagen content of bone, a colorimetric assay of hydroxyproline was performed using hydroxyproline standards. First, chloramine T was added to the bone hydrolysates and standards following incubation in the dark at room temperature (RT) for 20 minutes to initiate the reaction. The reaction was stopped by adding perchloric acid for 5 minutes at RT in the dark. Finally, p-dimethylaminobenzaldehyde was added and the samples and standards were incubated at 60°C for 20 minutes to produce a chromophore. After cooling down for 5 minutes at RT the absorbance of the bone hydrolysates and hydroxyproline standards was measured at a wavelength of 570 nm in a 96-well plate using a multimode microplate reader (VersaMax Tunable Microplate Reader; Molecular Devices, San Jose, CA, USA). For the fluorescence assay, quinine standards and hydrolysates of bone were measured in a 96-well plate using the multimode microplate reader at excitation of 355 nm and emission of 460 nm (Fluoroskan Ascent; Fisher Scientific GmbH, Schwerte, Germany). The total fAGEs are presented in nanograms of quinine fluorescence/milligrams collagen content.

Ultra-performance liquid chromatography tandem mass-spectrometry

Although fAGEs analyze the content of all fluorescent AGEs, ultra-performance liquid chromatography tandem mass-spectrometry (UPLC MS/MS) allows the determination of individual AGEs. Previously, a higher accumulation of CML was found in diabetic cortical bone tissue[20]; thus, here we focused on CML, N$^\varepsilon$-carboxyethyl-lysine (CEL), and N$^\delta$-(5-hydro-5-methyl-4-imidazolon-2-yl)-ornithine 1 (MG-H1). All three AGEs form by the reaction of glucose with free amino groups of bone protein (arginine or lysine side chains are the primary targets for these nonenzymatic modifications), are non-crosslinking AGEs and have been analyzed in cancellous bone tissue from the tibia.[45] Additionally, we assessed the cross-linking AGE pentosidine, which has been observed in urinary samples from patients with T2DM,[18] as well as in bone tissue from T1DM and T2DM patients.[19,21] Bone samples from the frozen femoral cross-sections (Fig. 1G; 18 controls and 16 DM cases) were mechanically pulverized

using a mortar. Subsequently, bone powders were washed with phosphate-buffered saline (0.15 mol/L NaCl in sodium phosphate buffer, pH 7.4), delipidated with chloroform/methanol (2:1, vol/vol) mixture during 24 hours at 4°C and demineralized with 0.5 mol/L EDTA in 50 mmol/L Tris buffer (pH 7.4) for 96 hours at 4°C. After centrifugation (4300g, 4°C, 20 minutes) the solvent was carefully removed with a Pasteur pipette.[45] For AGE analysis, the dried residue was prepared as described.[46] Pentosidine was analyzed with high-performance liquid chromatography (HPLC)-fluorescence as described.[47,48] Hydroxyproline (OH-Prol) was analyzed by UPLC MS/MS. In short, diluted hydrolysate was mixed with internal standard trans-4-hydroxy-L-proline-2,5,5-d$_3$ (D3-OH-Prol) and subsequently dried under a gentle stream of nitrogen at 70°C. The residue was dissolved in 1 mL water:acetonitrile (1:9, vol/vol) and injected on a hydrophilic interaction chromatography (HILIC) UPLC column. Solvent A was 10 mmol/L ammonium formate:acetonitrile (1:9, vol/vol) and solvent B was 10 mmol/L ammonium formate:acetonitrile (5:5, vol/vol). A linear gradient was started at 95% solvent A, which was changed to 60% solvent A within 2 minutes. After cleaning the column with 100% solvent B during 1.5 minutes the column was equilibrated for 4 minutes at the initial conditions. Injection volume was 0.2 μL (partial loop injection) at a column temperature of 45°C. OH-Prol and D3-OH-Prol were detected in multiple reaction monitoring electrospray positive mode (MRM-ESI) at a capillary voltage of 0.25 kV, a cone voltage of 25 V and a desolvation temperature of 600°C. Quantitation of OH-Prol was performed by calculating the peak area ratio of OH-Prol (MRM, 132.0 > 86.0) to the internal standard D3-OH-Prol (MRM, 135.0 > 89.0). AGE data were expressed as nmol AGE/μmol OH-Prol to reflect the raw data normalizing AGE data to measured hydroxyproline levels.

Statistical analysis

All statistical analyses were performed using GraphPad Prism 9 (GraphPad Software, San Diego, CA, USA). Data were tested for normality using the Kolmogorov-Smirnov test. Normally distributed data were tested for significant differences using two-sided t test, whereas not normally distributed data were tested by applying the Mann-Whitney U test. Data of several bone samples per individuals were averaged to obtain one mean value per individual. For comparison of differences between three groups to determine differences in elastic and inelastic fibril strain to tissue strain ratio, Dunnett's test was applied for normally distributed data and Dunn's test post hoc test for non-normally distributed data. Pearson correlation was performed to determine correlation of the fibril to tissue strain ratio to the elastic modulus. An alpha level below 0.05 was regarded as statistically significant. Data points above three times the interquartile range (IQR) of the upper limit of the range (75th percentile) or below three times the interquartile range from the lower limit of the interquartile range (the 25th percentile of the data) were defined as outliers.

Results

Bone mass and microarchitecture in DM using clinical imaging

The characteristics of the cohort are given in Table 1. Diabetes mellitus cases ($n = 17$) were compared to age- and BMI-matched control cases ($n = 18$) to assess differences between the diabetic

bone (combining T1DM and T2DM cases) and healthy control bone. To determine the clinically accessible bone status of the individuals, DXA was performed ex vivo on the 12th thoracic vertebra for analysis of the osteoporotic status based on areal BMD. The control and diabetic groups showed similar mean areal BMD values in both lateral and anterior-posterior scan directions. The diabetes mellitus group presented with a mean value for BMD measured in anterior-posterior direction of 0.85 mgHA/cm^2

Table 1. Sample Characteristics and Ex Vivo Clinical Parameters With Similar Results for All Control and DM Groups

Parameters	Co	DM
Samples		
n	18	17
Age (years)	69.3 ± 11.5	69.7 ± 12.1
BMI (kg/m^2)	26.4 ± 3.1	26.9 ± 4.7
DXA		
BMD AP (mgHA/cm^2)	0.93 ± 0.24	0.85 ± 0.12
BMD LAT (mgHA/cm^2)	0.66 ± 0.2	0.63 ± 0.12
HR-pQCT		
Ct.Ar (mm^2)	487.4 ± 85.8	503.9 ± 90.4
Ct.vBMD (mgHa/cm^3)	1065 ± 31.5	1049 ± 33.4
Ct.Th (mm)	6.81 ± 1.41	6.95 ± 1.35
Ct.Pm (mm)	102.2 ± 5.78	106.1 ± 8.47
Ct.Po (%)	1.85 ± 0.98	2.16 ± 1.27
Ct.Po.Dm (μm)	161.9 ± 32.1	178 ± 41

Sample characteristics and results of ex vivo bone mineral density of the 12th thoracic vertebra determined with DXA to analyze the osteoporotic status as well as HR-pQCT to determine clinical accessible bone microstructure were similar between control and diabetes mellitus cases. Data presented as mean ± SD. Unpaired two-sided *t* test was used for all parameters except for BMD LAT where Mann-Whitney *U* test was applied.

AP = anterior–posterior; BMD = bone mineral density; BMI = body mass index; C.Th = cortical thickness; Co = control; Ct.Ar = cortical area; Ct.Pm = cortical perimeter; Ct.Po.Dm = cortical pore diameter; Ct.Po = cortical porosity; Ct.vBMD = cortical volumetric bone mineral density; DM = diabetes mellitus; LAT = lateral.

compared to 0.93 mgHA/cm^2 in the control group. To assess ex vivo volumetric BMD and microarchitecture in cortical bone at the femoral mid-diaphysis, HR-pQCT was applied at a voxel size of 82 μm. Cortical volumetric BMD, microarchitecture, and porosity were similar between diabetes and control cases.

Nanoscale bone deformation by synchrotron-based imaging and materials testing

We aimed to determine changes in the mechanical behavior of bone at the collagen fibril length scale in femoral mid-diaphyseal bone samples (Fig. 1A). Thin sections of bone were loaded in tension until failure at a synchrotron facility (Fig. 1B,C). During tensile testing, the sample was exposed to synchrotron X-rays, which are sensitive to the nanoscale mineralized collagen fibril structure such that mechanical deformation can be measured (Fig. 1C). Strain in the mineralized collagen fibrils was measured based on normalized changes in the position of the first-order diffraction peak and compared to the macroscopic tissue strain in the entire bone sample based on normalized changes in sample length during tensile testing measured through marks on the sample's surface. Slopes of linear regressions in the elastic region were defined below a tissue strain of 0.55% as reported[17] and were analyzed to determine the fibril to tissue strain ratio (Fig. 1D). Here, the analysis revealed a significantly lower fibril to tissue strain ratio based on the slopes of the fibril strain-tissue strain curve in the elastic portion of the graphs for the diabetes group (Fig. 2A, *p* = 0.0046). The fibril to tissue strain ratio describes the proportion of tissue-level strain transferred to the fibril level. The mean values of fibril deformation determined with SAXS with standard deviation plotted over the tissue strain from tensile testing for control and DM group are plotted in Fig. 2B. Additionally, the analysis of slopes of the fibril strain-tissue strain curves in the inelastic (ie, irreversible) range, following the elastic/inelastic transition at 0.55%, revealed a significantly lower fibril to tissue strain ratio in diabetes mellitus (*p* = 0.0020; Fig. 2C) compared to age- and BMI-matched control cases.
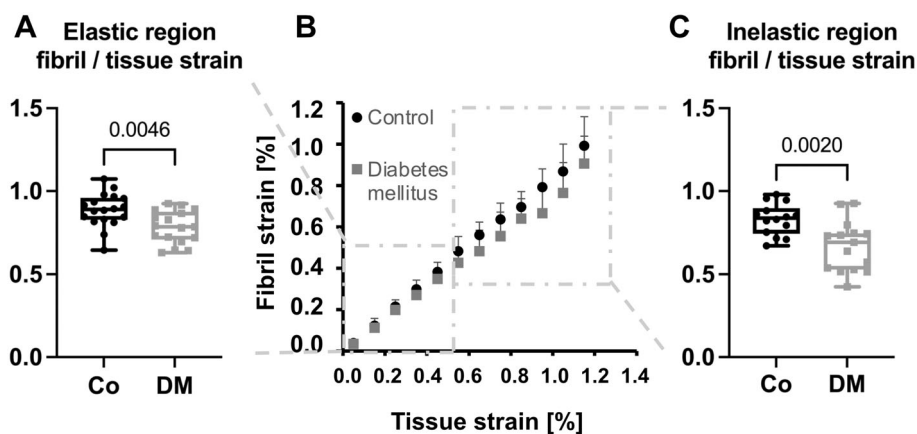
Fig. 2. Lower fibril deformation in DM measured with synchrotron small-angle X-ray scattering. (*A*) Fibril to tissue strain ratio in the elastic region. (*B*) Fibril strain plotted versus tissue strain (mean value with standard deviation). (*C*) Inelastic region of DM cases compared to age- and BMI- matched control cases. Unpaired two-sided *t*-test was used for all parameters. Data is shown with median and interquartile range (25th to 75th percentile). Whiskers denote maximum and minimum values and individual data points are shown as dots displaying the average of several tests within one donor. Co = control; DM = diabetes mellitus.

Mineralization patterns in DM

To assess whether mineral differences in bone matrix composition contributed to changes in the collagen fibril deformation, patterns of mineralization were assessed with qBEI. Here, the grayscale is proportional to the calcium weight percentage (Fig. 3A), higher mineralized areas appear brighter and lower mineralized areas appear darker, which provides a distribution
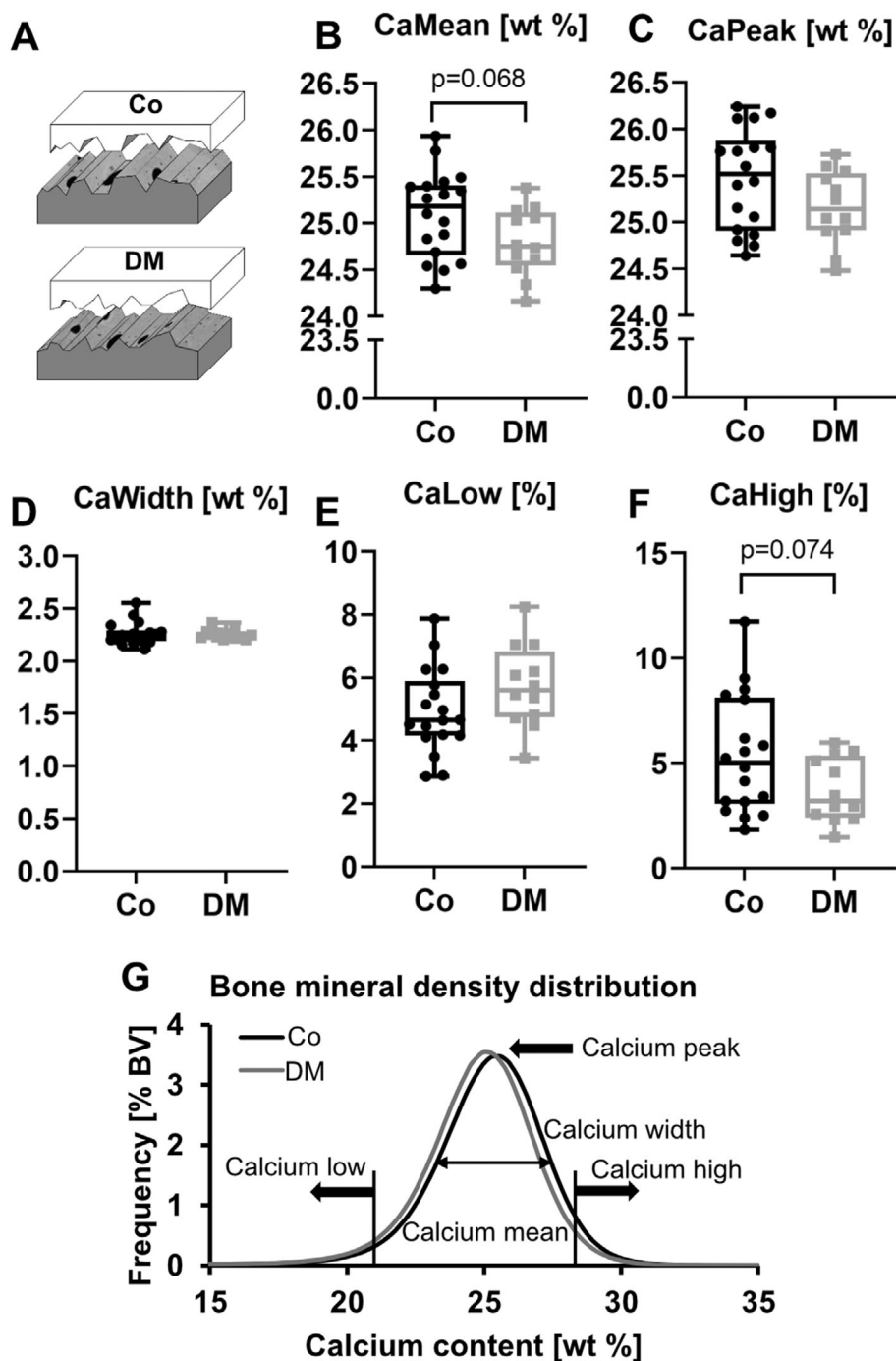

Fig. 3. Diabetes samples show a tendency toward lower mineralization along with fewer high mineralized bone packets. (A) Schematic images of tested bone samples displaying the fracture site for control and DM cases. (B) Mean calcium weight percentage in diabetes samples compared to control. (C) Peak calcium weight percentage for both groups. (D) Calcium width weight percentage reflects the mineralization heterogeneity. (E) Calcium low indicates the percentage of bone area with low mineralized bone packets, whereas (F) the calcium high represents the percentage bone area of high mineralized bone packets. (G) Bone mineral density distribution histograms of control (black) and diabetes mellitus (gray) cases. Two-sided unpaired t-test was applied except for CaWidth where Mann-Whitney U test was used. Data is shown with median and interquartile range (25th to 75th percentile). Whiskers denote maximum and minimum values and individual data points are shown as dots. Co = control; DM = diabetes mellitus.

of the mineral content within the bone section. This mineral distribution is described in terms of (i) the average calcium weight percentage, (ii) the most frequent calcium weight percentage value found in the analyzed region, (iii) the heterogeneity of the calcium weight percentage distribution, and (iv) the proportion of low and high mineralized bone areas. The analysis points to an overall lower mineralization in DM cases through the

tendency for lower average calcium content (calcium mean) compared to controls ($p = 0.068$; Fig. 3B). The most frequent calcium weight percentage (calcium peak) and the heterogeneity of mineralization distribution (calcium width) within the bone tissue of both groups did not differ (Fig. 3C,D). Although the proportion of bone area with low mineralized bone packets was similar (Fig. 3E), the percentage of bone area with high
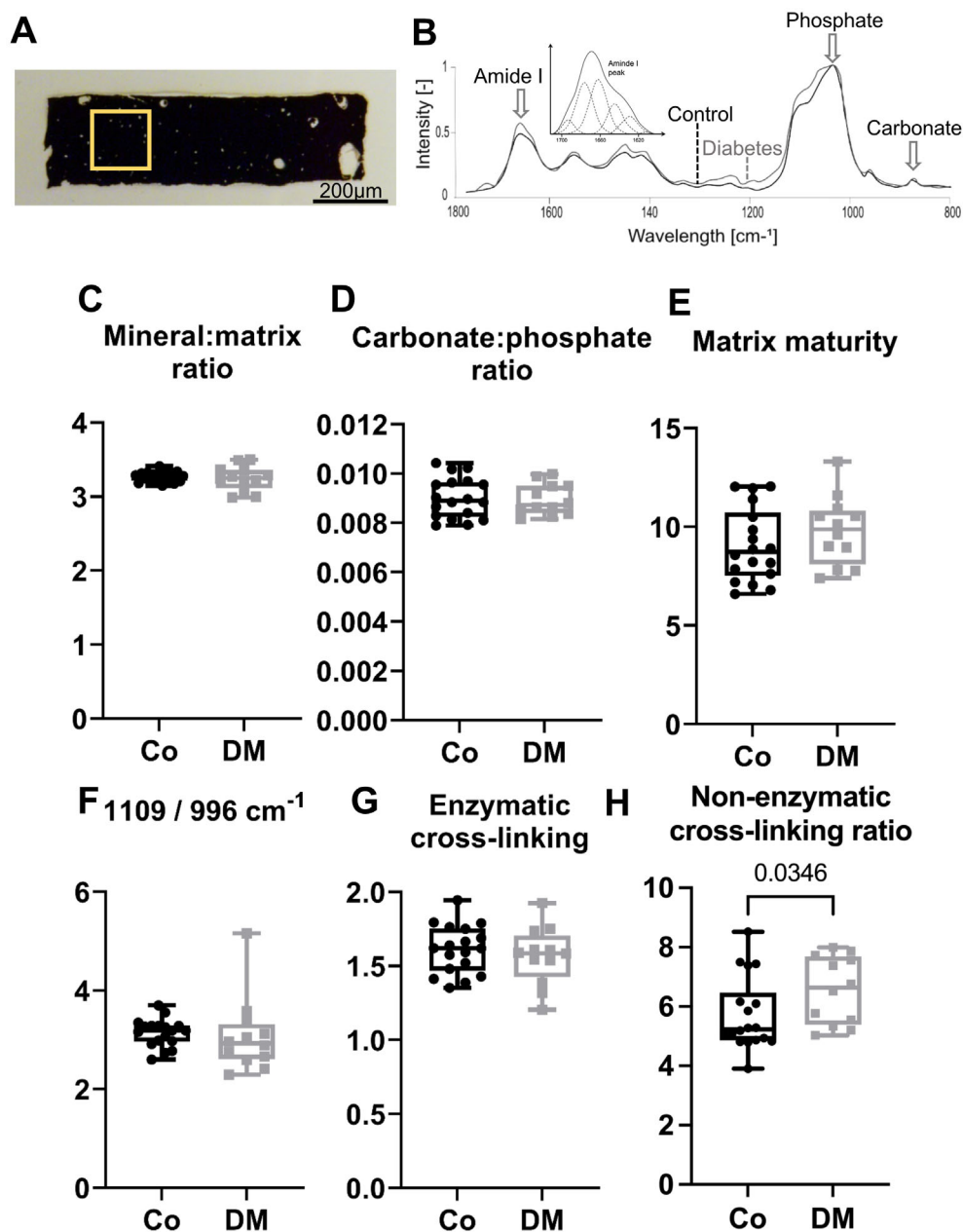

Fig. 4. Spectroscopy analysis of bone matrix composition and cross-linking. (A) Microscopy image of von Kossa stained bone sample at the fracture site with labeled region of interest for spectroscopy analyses. (B) Representative FTIR spectra of control and DM cases including subpeak fitting for the amide I peak. (C) Mineral-to-matrix and (D) carbonate-to-phosphate ratio determined for DM and control cases. (E) Matrix maturity and (F) ratio of poorly crystalline apatites (phosphate subpeak 1109 cm^{-1}) over PO$_4^{-3}$ in apatitic environment (phosphate subpeak 996 cm^{-1}) in DM and control cases. (G) Enzymatic cross-linking ratio and (H) the nonenzymatic crosslinking ratio as surrogate for collagen quality. For all parameters, except for the nonenzymatic crosslinking ratio where Mann-Whitney U test was used, unpaired two-sided t test was applied. Data is shown with median and interquartile range (25th to 75th percentile). Whiskers denote maximum and minimum values and individual data points are shown as dots. Co = control; DM = diabetes mellitus.

mineralized bone packets showed a tendency to be lower in DM compared to control cases ($p = 0.074$; Fig. 3F). This contributes to a tendency of lower average calcium weight percentage shown by a slight shift of diabetic BMDD histograms to the left (Fig. 3G).

Collagenous and mineral composites in diabetic bone matrices

To measure bone composition with high sensitivity to both mineral and organic constituents, FTIR was performed on the fracture site of the tested beams on an area of 150 μm × 150 μm (Fig. 4A). From these FTIR spectra, ratios of peak areas are associated with different aspects of bone composition (Fig. 4B). (i) Mineral-to-matrix ratio, which is a measure of mineral per amount of collagen within the bone tissue, and (ii) the carbonate-to-phosphate ratio, which is related to bone remodeling rate and bone turnover, were similar in both groups (Fig. 4C, D). (iii) Mineral crystallinity, which is obtained via peak-fitting based on the phosphate peak and is an overall measure of the mineral crystal size; the mineral crystallinity; and (iv) the mineral maturity, were both similar in diabetes mellitus and control cases indicating no changes in these mineral properties. (v) The ratio of poorly crystalline apatites (phosphate subpeak 1109 cm^{-1}) over PO$_4$$^{-3}$ in apatitic environment (phosphate subpeak 996 cm^{-1})[44] describes maturation processes of crystalline

apatites and was similar in both groups (Fig. 4E); (vi) the matrix maturity (Fig. 4F); and (vii) the enzymatic cross-linking ratio, describing enzymatic cross-linking, which occur by posttranslational modifications of the collagen fibrils stabilizing the collagenous matrix, did not differ between both groups (Fig. 4G). (viii) The nonenzymatic cross-linking ratio, describing nonenzymatic cross-linking which form through the reaction of sugar with bone matrix proteins, was significantly higher in the diabetes mellitus group compared to the control group ($p = 0.034$; Fig. 4H).

AGE content in diabetic bone matrices

To determine AGE accumulation in bone tissue, we measured the exact content of three specific AGEs using mass spectrometric quantitation: CML, N$^\varepsilon$-carboxyethyl-lysine (CEL), N$^\delta$-(5-hydro-5-methyl-4-imidazolon-2-yl)-ornithine 1 (MG-H1), and pentosidine. All AGEs form by the reaction of glucose with free amino groups of bone protein (arginine or lysine side chains are the primary targets for these nonenzymatic modifications). CML, CEL, and MG-H1 are non-crosslinking AGEs whereas pentosidine is a cross-linking AGE (Fig. 5A). Here, we found significantly higher levels of CML ($p = 0.0416$; Fig. 5B), whereas CEL presented with no differences between the groups (data not shown). MG-H1 is an arginine-derived AGE and was significantly higher in the DM
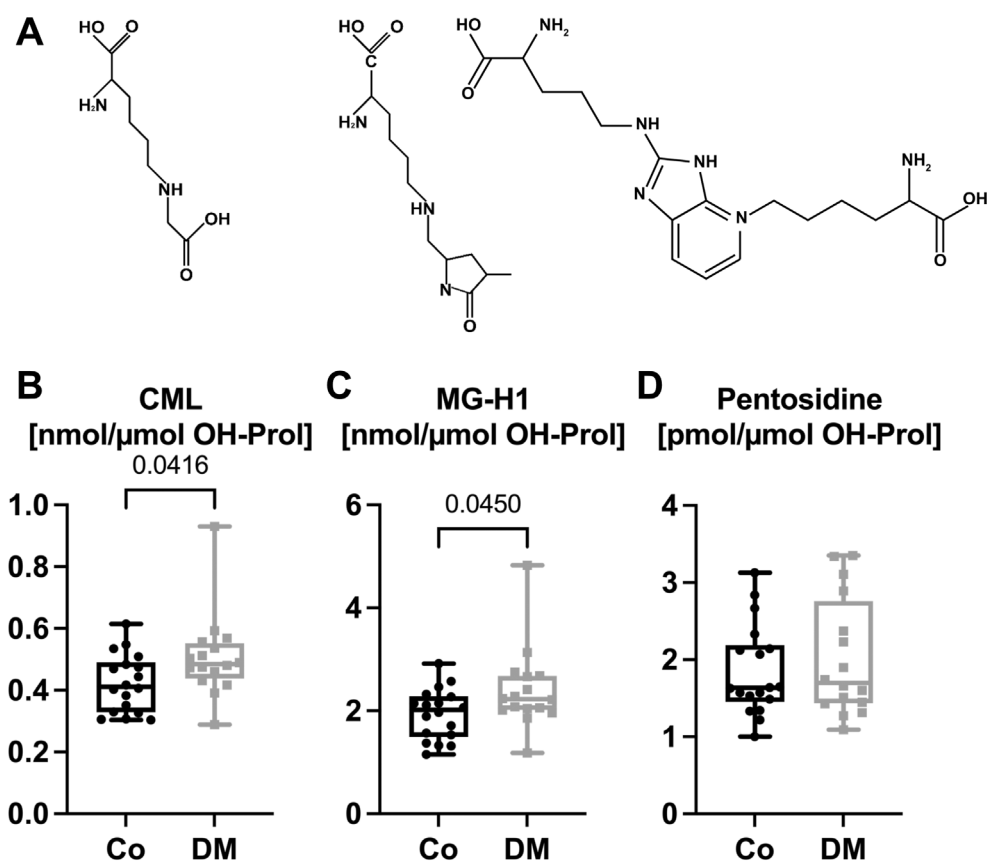
Fig. 5. Mass spectrometry assessment of advanced glycation end-product content. (A) Structure formula for N$^\varepsilon$-carboxymethyl-lysine (CML), N$^\delta$-(5-hydro-5-methyl-4-imidazolon-2-yl)-ornithine 1 (MG-H1), and pentosidine. (B) Results for CML, (C) MG-H1, and (D) pentosidine content normalized to hydroxyproline content. Two-sided unpaired t test was applied for statistical analysis. Data is shown with median and interquartile range (25th to 75th percentile). Whiskers denote maximum and minimum values and individual data points are shown as dots. Co = control; DM = diabetes mellitus.

group compared to age- and BMI-matched controls ($p = 0.045$; Fig. 5C). The cross-linking AGE pentosidine presented with similar content in both groups (Fig. 5D). After removal of one outlier within the DM group, CML and MG-H1 presented with a tendency to higher AGE accumulation in DM compared to control cases ($p = 0.07$ and $p = 0.08$, respectively).

Bone quality indices in T1DM and T2DM

DM types T1DM and T2DM present with pathophysiological differences. Therefore, the DM group was differentiated into T1DM cases ($n = 6$) and T2DM cases ($n = 11$) and compared to the control group. Although T1DM individuals were all treated with insulin, the T2DM individuals were either treated with oral antidiabetics ($n = 6$) or insulin ($n = 3$). Subgrouping maintained similar distribution of age and BMI between subgroups (Table 2). Although presenting without statistically significant differences, it is noticeable that the T2DM group presented with the lowest mean values for vertebral BMD measured in anterior-posterior direction with DXA as well as for femoral cortical BMD measured

with HR-pQCT. Specifically, the T2DM group showed a mean value of 0.83 mgHA/cm^2 whereas the control group presented with 0.93 mgHA/cm^2 and the T1DM group with 0.88 mgHA/cm^2 for areal BMD. Cortical volumetric BMD in T2DM was 1043 mgHA/cm^3 compared to 1062 mgHA/cm^3 in control and 1061 mgHA/cm^3 in T1DM. The mineralization, AGE accumulation, and compositional properties analyzed with qBEI and FTIR were similar between all three groups and are presented in Table 2.

Bone quality changes in T1DM and T2DM

As it responds to mechanical forces, bone passes through an elastic region, where the changes in the tissue are reversible, into an inelastic region, where plastic deformation leads to permanent changes in the tissue. Cortical bone tissue in both T1DM and T2DM present with altered patterns of fibril deformation. Figure 6A shows that in the elastic region, the fibril to tissue strain ratio is significantly lower in T2DM compared to control ($p = 0.0154$). A similar pattern is observed for the inelastic region, as shown in Fig. 6B, in which the fibril to tissue strain ratio tends

Table 2. Ex Vivo Clinical and Bone Material Quality Parameters with Similar Results for All Three Groups

Parameters	Co	T1DM	T2DM
Samples			
n	18	6	11
Age (years)	69.3 ± 11.5	61.3 ± 14.6	74.3 ± 7.9
BMI (kg/m^2)	26.4 ± 3.1	26.9 ± 5.1	26.2 ± 6.6
DXA			
BMD AP (mgHA/cm^2)	0.93 ± 0.24	0.88 ± 0.1	0.83 ± 0.13
BMD LAT (mgHA/cm^2)	0.66 ± 0.2	0.62 ± 0.11	0.63 ± 0.12
HR-pQCT			
Ct.Ar (mm^2)	487.4 ± 85.8	569 ± 100	467.7 ± 64.4
Ct.vBMD (mgHa/cm^3)	1065 ± 31.5	1061 ± 42.6	1043 ± 27.7
Ct.Th (mm)	6.81 ± 1.41	7.91 ± 1.47	6.42 ± 1.00
Ct.Pm (mm)	102.2 ± 5.78	107.7 ± 5.68	105.2 ± 9.89
Ct.Po (%)	1.85 ± 0.98	2.16 ± 1.77	2.08 ± 1.02
Ct.Po.Dm (μm)	161.9 ± 32.1	152.4 ± 25.9	192.4 ± 41.6
qBEI			
CaMean (wt%)	25.1 ± 0.46	24.64 ± 0.44	24.91 ± 0.29
CaPeak (wt%)	25.47 ± 0.54	25.00 ± 0.49	25.27 ± 0.30
CaWidth (wt%)	2.26 ± 0.11	2.27 ± 0.06	2.247 ± 0.04
CaHigh (%)	5.37 ± 2.79	3.36 ± 1.86	3.98 ± 1.34
FTIR			
Mineral matrix ratio	3.27 ± 0.07	3.24 ± 0.18	3.26 ± 0.17
Carbonate phosphate ratio	0.0090 ± 0.0008	0.0089 ± 0.0007	0.0089 ± 0.0006
Crystallinity	0.83 ± 0.14	0.78 ± 0.14	0.85 ± 0.12
Mineral maturity	0.94 ± 0.1	0.93 ± 0.10	0.96 ± 0.1
Matrix maturity	9.05 ± 1.85	9.12 ± 1.59	10.29 ± 1.78
Enzymatic cross-link ratio	1.61 ± 0.16	1.53 ± 0.27	1.59 ± 0.14
AGEs			
fAGEs (ng quinine/mg col)	185.3 ± 52.6	196.7 ± 58.0	186.7 ± 64.5
CEL (nmol/μmol OH-Prol)	0.182 ± 0.067	0.232 ± 0.148	0.211 ± 0.057
Pentosidine (pmol/μmol OH-Prol)	1.848 ± 0.589	1.993 ± 0.831	2.029 ± 0.776

Results of ex vivo bone mineral density of the 12th thoracic vertebra determined with DXA to analyze the fracture risk and osteoporotic status in line with the cohort characteristics. Microstructural data of femoral cross-sections obtained by HR-pQCT reflecting the bone status in a clinical setting. Bone material quality indices of the mineral and collagen phase in the bone matrix, which contribute to bone's resistance to fracture (i.e., toughness), fluorescent AGEs and CEL content for T1DM, T2DM, and age- and BMI-matched controls. Data presented as mean ± standard deviation.

AGE = advanced glycation end-product; AP = anterior–posterior; BMD = bone mineral density; BMI = body mass index; C.Th = cortical thickness; CaHigh = calcium high; calcium peak; CaMean = calcium mean; CaPeak = calcium peak; CaWidth = calcium width; CEL = N^e-(carboxyethyl-lysine); Co = control; Ct.Ar = cortical area; Ct.Pm = cortical perimeter; Ct.Po.Dm = cortical pore diameter; Ct.Po = cortical porosity; Ct.vBMD = cortical volumetric bone mineral density; fAGE = fluorescent advanced glycation end-product; FTIR = Fourier transform infrared spectroscopy; LAT = lateral; qBEI = quantitative backscattered electron imaging.
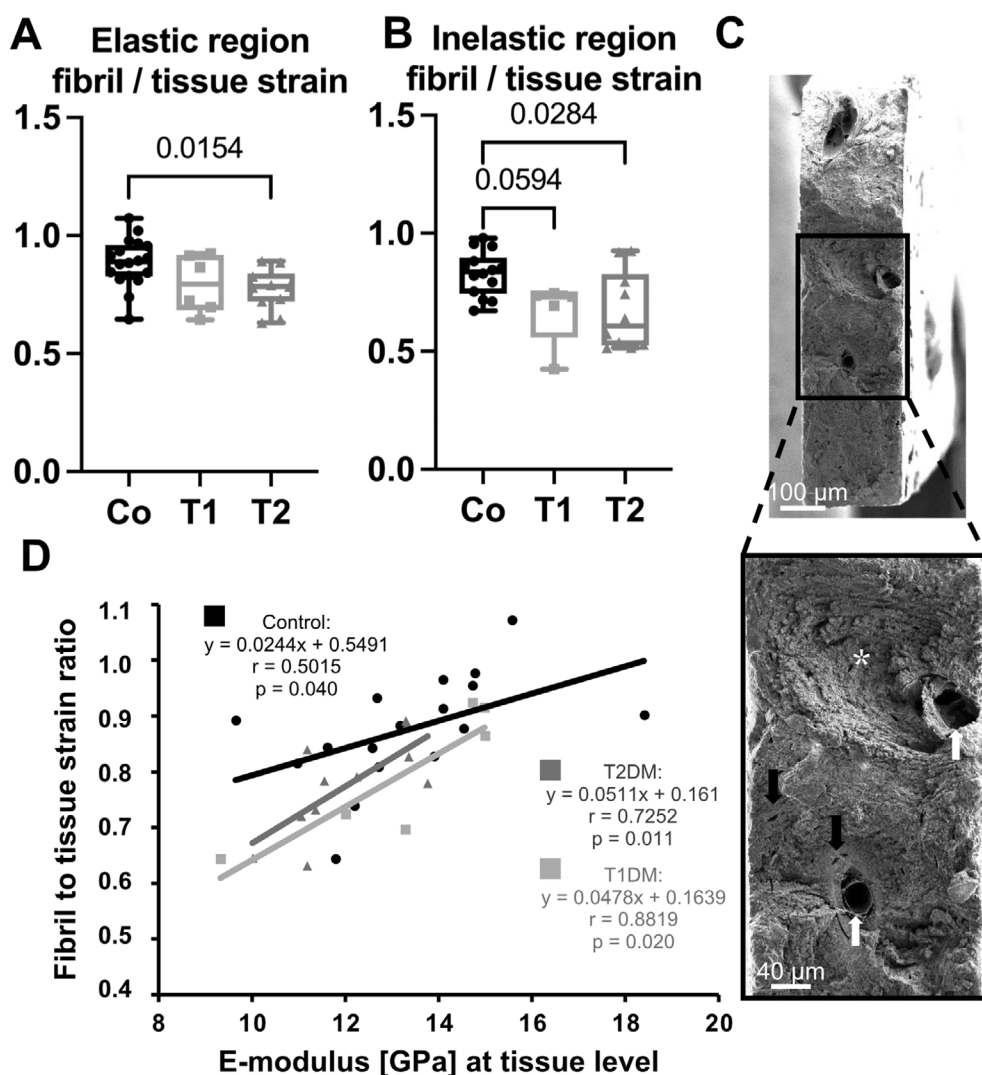
Fig. 6. Dimorphic mechanisms contribute to lower fibril strain in T1DM and T2DM. (*A*) Fibril over tissue strain in the elastic and (*B*) inelastic region in T1DM, T2DM, and matched cortical bone tissue. (*C*) Scanning electron microscopy images of the fracture surface showing Haversian canals (white arrows) and osteocyte lacunae (black arrows) as well as lamellar structure of osteons (asterisk) of a bone sample from a diabetic individual. (*D*) Fibril to tissue strain ratio significantly correlated with elastic modulus showing a twofold lower slope in control cases (dots) compared to T1DM (squares) and T2DM cases (triangles). Dunnett's test was performed to compare elastic fibril to tissue strain ratio and Dunn's test to compare inelastic fibril to tissue strain ratio in T1DM and T2DM to control. Pearson correlation was applied to correlate the fibril to tissue strain ratio with the elastic modulus. Data is shown with median and interquartile range (25th to 75th percentile). Whiskers denote maximum and minimum values and individual data points are shown as dots displaying the average of several tests within one donor. Co = control; T1 = type 1 diabetes mellitus; T2 = type 2 diabetes mellitus.

to be lower in T1DM ($p = 0.0594$) and is significantly lower in T2DM ($p = 0.0284$), each as compared to control. Scanning electron microscopy images of the fracture site of a diabetic bone sample following tensile testing highlights the osteonal structure of the cortical bone with collagen lamellae surrounding a Haversian canal and osteocyte lacunae within the bone matrix (Fig. 6C). Fibril to tissue strain ratio in the elastic region has a linear relationship with the elastic modulus, which correlates significantly in all three groups (control: $p = 0.040$, T1DM: $p = 0.020$, T2DM: $p = 0.011$; Fig. 6D).

Clinical BMD is often described to be normal or lower in patients with T1DM, because this is different from T2DM cases, it is suggested to be unique feature of T1DM.[8] To determine

diabetes type–specific changes that lead to lower collagen deformation, we focused on mineral parameters in T1DM and compared these to control cases. By this, we found a tendency to lower average mineralization degree in T1DM compared to control group ($p = 0.0629$; Fig. 7A) which was accompanied by a significantly higher percentage of bone area with low mineralized bone packets ($p = 0.0415$; Fig. 7B). Furthermore, a lower ratio of poorly crystalline apatites over PO_4^{-3} in the apatitic environment in T1DM compared to control cases analyzed with spectroscopy was shown ($p = 0.026$; Fig. 7C).

It is assumed, that in T2DM AGE accumulation play a major role in increased fracture risk. In T2DM, we observed a tendency to higher content of non-cross-linking AGE CML ($p = 0.0709$;
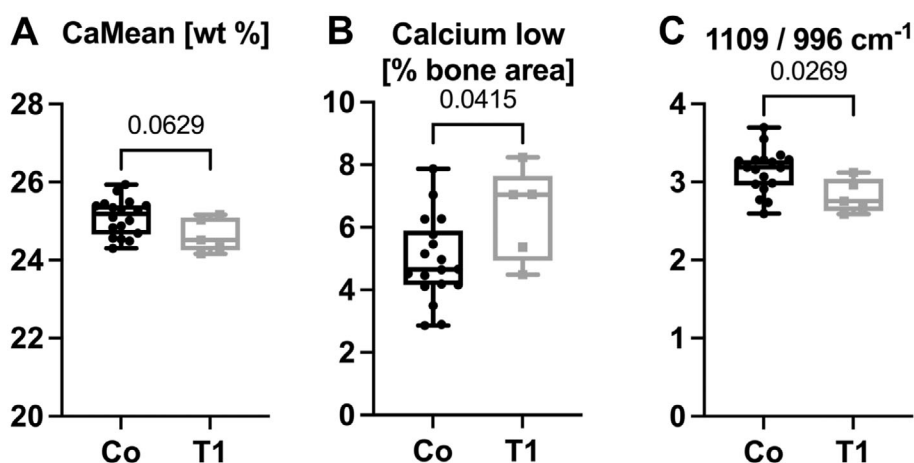
Fig. 7. In T1DM, mineralization related parameters were analyzed and compared to the control group. (*A*) The average calcium content in T1DM tended to be lower compared to control cases, which was due to (*B*) higher amount of bone packages with low mineralized bone tissue. (*C*) The ratio of poorly crystalline apatites over PO_4^{-3} in an apatitic environment was lower in T1DM cases compared to control cases. Two-sided unpaired *t* test was applied for statistical analysis. Data is shown with median and interquartile range (25th to 75th percentile). Whiskers denote maximum and minimum values and individual data points are shown as dots. Co = control, T1 = type 1 diabetes mellitus.
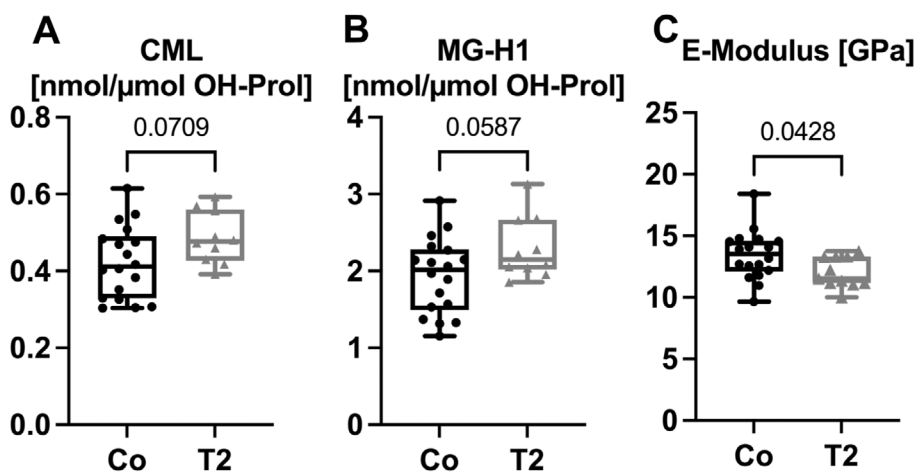
Fig. 8. In T2DM, the E-modulus and advanced glycation end-products were analyzed. (*A*) Advanced glycation end-product analysis showed a tendency in higher CML and (*B*) MG-H1 accumulation in T2DM compared to healthy, age- and BMI-matched individuals. (*C*) A significantly lower E-modulus was observed in individuals with T2DM based on tensile testing. Two-sided unpaired *t* test was applied for statistical analysis. Data is shown with median and interquartile range (25th to 75th percentile). Whiskers denote maximum and minimum values and individual data points are shown as dots. Co = control, T2 = type 2 diabetes mellitus.

Fig. 8*A*) and MG-H1 ($p = 0.0587$; Fig. 8*B*). To determine whether this potential change may influence biomechanical properties of the bone we analyzed the elastic modulus in T2DM individuals compared to controls and found a significantly lower elastic modulus in T2DM ($p = 0.0428$; Fig. 8*C*).

Discussion

Diabetes mellitus is a metabolic disease that can be accompanied by a higher fracture risk,[49,50] the resulting disease is defined as "diabetic bone disease" and its underlying mechanisms are still unclear.[15] Here we have used a combination of clinical indices and high-resolution bone quality assessments to investigate the origin of fracture risk in diabetes mellitus.

Challenges for clinical imaging to capture bone quality changes in DM

Our ex vivo clinical analysis using DXA (2D) and HR-pQCT (three-dimensional [3D]) showed that differences between male DM and age-/BMI-matched controls are challenging to identify when standard clinical osteodensitometry technologies are used to

evaluate fracture risk.[51] Here, we focus on male individuals to rule out sexual dimorphism derived from geometry and interferences with estrogens versus androgens because sex-related factors differentially affect bone metabolism, especially at older ages. The DM group (combined T1DM, T2DM) showed a lower mean vertebral aBMD in the anterior-posterior direction (not statistically significant). After stratification by diabetes types, this difference seems to arise from the T2DM group, which surprisingly presented with the lowest values for vertebral aBMD measured with DXA as well as for femoral Ct.vBMD using HR-pQCT, despite the assumption that T2DM present with normal or high BMD. This can be due to two reasons: (i) the sample size might be too low to determine significant changes within the groups; and (ii) the samples analyzed here were BMI-matched and therefore, obesity does not seem to contribute to BMD in T2DM group. Cortical porosity has been proposed to be linked to increased fracture susceptibility in T2DM patients in previous clinical studies[12,32]; here, we focused on samples with similar cortical porosity compared to control cases. Certainly, cortical porosity plays a pivotal role in fracture risk; however, bone material quality in the diabetic mineralized tissue may be affected independent of cortical porosity.

Impaired mechanical response in diabetic bone at the collagen level

Bones have a multiscale structure and the small length scale of the collagen fibril (10–100s of nanometers) plays an important role in deformation and energy absorption in response to mechanical challenges. It is supposed that when bone is mechanically challenged, the more that macro level strain is transferred into deformation, at the collagen fibril scale, the less that strain causes damage at the higher length scales. During tensile testing, the mineralized collagen fibrils deform by stretching of molecular bonds and the load experienced by the fibrils is transferred to and between the mineral crystals which sustain high loads[17,52-54] creating an inherent toughness. This physiologically inherent toughness of bone material determines fracture susceptibility. In our study, we show that toughening mechanisms are impaired at the fibrillar length scale in individuals with DM. Specifically, the changes of the collagen fibrils for a given tissue strain are lower in the diabetes samples indicating less deformation or smaller extension of the collagen fibrils in response to tensile forces. The lower deformation at the nanoscale in DM might result in more load being transferred to the mineral platelets[54] or in microcracks at high length-scales. Similar observations were made in obese UCD-T2DM rats.[55] At the tissue level, we did not observe differences in the elastic modulus between the control and DM group based on tensile tests. Although it has been shown that fracture toughness in diabetic mice can be predicted by pentosidine (predicting the loss of toughening effect) and CML (predicting the maximum toughness in bone),[26] we can only postulate that the lower collagen fibril deformation in combination with higher CML accumulation induces reduced toughness of diabetic bone tissue.

Impaired matrix composition in DM

The differences in fibrillar-level mechanical behavior between control and diabetes cases should arise due to physical differences in bone matrix composition or nanoscale structure. The mineral component of bone contributes to its mechanical behavior by reinforcing the collagen matrix and providing greater modulus and strength. During bone remodeling older, highly mineralized bone matrix is resorbed and substituted by new bone matrix in the form of type-I collagen-rich osteoid, which slowly increases in HA content during mineralization. With aging, the proportion of highly mineralized human cortical bone further increases at the expense of less mineralized bone[56] due to an imbalanced and impaired bone remodeling. Although the mineral contributes to bone stiffness, the collagenous matrix contributes to the capacity of bone to absorb energy (toughness). Age- and diabetes-related modifications to the organic components may thereby also affect its deformation capability. One of the posttranslational modifications is the formation of AGEs. A variety of different AGEs exist; the cross-linking AGE pentosidine and non-cross-linking N^ε-carboxymethyl-lysine (CML) are the most studied AGEs in bone. Although the higher nonenzymatic cross-linking ratio determined with FTIR in DM compared to control cases points toward changes in the cross-linking environment of diabetic bone, the exact content of the full spectrum of AGEs present within the diabetic bone matrix are still unknown. CML is a nonfluorescent and non-crosslinking AGE, which has recently been shown to be more abundant than pentosidine in bone tissue.[23] CML is also present in processed food and therefore ingested by our daily food intake. AGEs accumulate in the diabetic bone matrix, which can evolve due to glycosylation of proteins[57,58] and modify the collagen fibril properties of the bone matrix, resulting in poor collagen network stability.[59] Here, we found a significantly higher ratio of nonenzymatic crosslinking ratio. Higher nonenzymatic crosslinking ratio was also shown by Sihota and colleagues[60] in trabecular bone from femoral heads of male and female patients undergoing joint replacement surgery following hip fractures. In addition, a lower enzymatic crosslinking ratio and a lower mineral-to-matrix ratio in the diabetic group were found in comparison to the nondiabetic group. Our other analyzed FTIR parameters showed no significant difference between the two study groups. This may be due to a lower sample size used in our study. However, Sihota and colleagues[60] have also focused on different bone regions and compartments, which may also influence the FTIR indices relating to collagen and mineralization properties. Of note, cortical bone tissue is less metabolically active than trabecular bone tissue. Furthermore, Sihota and colleagues[60] have analyzed bone tissue obtained from patients with fractures. FTIR indices reflecting the matrix properties of fractured bone may vary from those obtained from tissue not related to fractures. Finally, our samples were fixed and embedded, which may have a potential effect on the bone tissue and specifically on bone collagen, while the samples used in Sihota and colleagues'[60] study were freeze-dried bone sections. The herewith presented study was powered to detect differences in collagen fibril deformation, although other techniques assessing bone material properties in diabetic bone matrix might have required greater sample sizes. Conclusively, additional significant differences might be observable with higher-powered studies. Such studies are needed to further characterize the effects of the diabetic bone disease with special emphasis on bone material quality parameters and fractures (Table 2).

Additionally, to a higher nonenzymatic crosslinking ratio a significantly higher amount of non-crosslinking AGEs CML and MG-H1 in DM. Although it is not yet a possibility to capture the full spectrum of AGEs present in bone, this is a very important result because it demonstrates that non-crosslinking AGEs may reduce collagen fibril deformation through unknown mechanisms, such as drag or distortion of the collagen fibril array. The crosslinking

AGE pentosidine presented with similar content in both groups. Higher urine levels of pentosidine are associated with incident clinical fracture and prevalent vertebral fractures in diabetic patients independent of BMD, while urinary pentosidine levels were similar in patients with and without diabetes.[18] As a cross-linking AGE, the formation of pentosidine requires the presence of two collagen fibrils with specific amino acid residues in vicinity. This requirement is rather rare, which is why non-crosslinking AGEs, such as CML and MG-H1, which form solely with amino acids of one collagen fibril, are believed to form more frequently.[45] Higher pentosidine content in bone tissue was only found in trabecular bone from the femoral neck of T2DM patients with osteoarthritis[19] and in trabecular bone from iliac crest biopsies from T1DM patients with prior fragility fracture.[21] Higher blood serum CML levels are linked to increased fracture risk[61] and associated with hyperglycemia and fracture risk in older men[62] as well as with increased fracture risk in female T2DM patients independent of BMD.[24] Our findings underline the previously suspected relevance of AGEs in diabetes mellitus, link it to nanoscale mechanical behavior, and further support the importance of non-crosslinking AGEs in bone material quality impairments.

T1DM presents with more low mineralized bone packets and a lower ratio of poorly crystalline apatites over PO_4^{-3} in apatitic domains

T1DM and T2DM display pathophysiological differences which lead to the assumption that bone is affected by the two DM types in distinct ways.[63] We differentiated the two DM types and focused on mineralization parameters in T1DM cases compared to control cases. Here, we observed a tendency to lower average calcium weight percentage in T1DM derived from higher amounts of low mineralized bone packets, which originate from a delay in mineralization. The interpretation of delayed mineralized is supported by FTIR data, where a lower ratio of the 1109/996 peaks was observed. The peak 1109 cm^{-1} has been described as a measure of poorly crystalline apatite and 996 cm^{-1} as PO_4^{-3} in an apatitic environment[44]; however, to our knowledge, the peak area ratio has not been previously evaluated. In T1DM, new bone formation with bone packets of low mineral content seems unlikely due to the low bone turnover associated with DM. Thus, looking at the crystalline maturation process, poorly crystalline apatites, which are composed of an apatitic domain surrounded by a hydrated layer, incorporate PO_4^{-3} ions from the hydrated layer into the apatitic domain.[64] Therefore, we interpret that a lower ratio of 1109/996 cm^{-1} either requires fewer poorly crystalline apatites and / or a higher amount of PO_4^{-3} in an apatitic environment, which both seem to occur during the maturation process of poorly crystalline apatites. Thereby, a lower ratio of 1109/996 cm^{-1} suggests more mature crystalline apatite in T1DM. The combination of more low mineralized bone packets through qBEI with more mature crystals determined with FTIR suggests a higher mineral heterogeneity in T1DM individuals. While this interpretation is based on literature describing individual peaks and the maturation process of crystalline apatites, further validation of the 1109/996 ratio is required in future studies addressing fracture risk characteristics.

Farlay et al., described an overall higher degree of mineralization in iliac-crest biopsies from T1DM patients with prior fracture compared to controls and T1DM patients without fractures.[21] When comparing these findings, it should be considered that study cohorts, skeletal sites and techniques differed. Moreover, our results are in line with the general assumption of a lower BMD in T1DM patients reported in clinical studies.[49]

Regarding non-enzymatic cross-linking in the collagen phase the T1DM group presented with similar mean values for the nonenzymatic crosslinking ratio measured with FTIR compared to the T2DM group (6.598 ± 1.384 versus 6.531 ± 1.044, respectively). As such, nonenzymatic cross-linking in cortical bone might also play a role in T1DM bone fragility, which is in agreement with significantly higher pentosidine content in trabecular bone of iliac-crest biopsies in patients with T1DM and fractures compared to controls.[21] Although these data indicate a higher AGE accumulation, the fAGE analysis results confirm other studies showing marginal or no differences in fAGEs in diabetic bone.[19,20,22] However, other studies have shown a trend towards higher fAGE accumulation in cortical bone from the femoral neck.[22] In trabecular bone of diabetic postmenopausal women undergoing total hip arthroplasty a 1.5-fold higher fAGE level was found.[65] In addition, in diabetes patients higher fAGE levels were analyzed in bone tissue from femoral heads,[60] suggesting that not only the skeletal site but also the bone compartment may affect the degree of fAGE accumulation in diabetes. We did not observe differences in fluorescent AGE pentosidine in DM compared to control groups, whereas in other studies higher pentosidine content was found in trabecular bone from the femoral neck of male patients undergoing total hip arthroplasty using HPLC.[19] Comparison of AGE levels reported in studies presents a challenge, because normalization of the assessed AGE using HPLC may vary through different conversion of measured hydroxyproline values into collagen content. Nevertheless, age-related increases in AGE accumulation have been shown to impair the fracture toughness of cortical bone[16] and seem to be further increased in diabetes mellitus contributing to the presented higher fracture risk.

T2DM showed a lower elastic modulus accompanied by higher CML content

In T2DM bone, we focused on AGE accumulation and potential effects on the elastic modulus and found that less fibril deformation in T2DM is related to a tendency to higher CML and MG-H1 accumulation and to lower elastic modulus. The lower elastic modulus in T2DM bone implies less resistance to reversible deformation at the tissue level. The elastic modulus is linked to the mineralization of bone. There is a positive correlation between fibril-to-tissue strain ratio and elastic modulus, which is more severe in T2DM: samples with a lower elastic modulus (ie, lower degree of mineralization) have less fibril deformation and vice versa, samples with higher elastic moduli (ie, higher degree of mineralization) have greater fibril deformation. This signifies, when the overall resistance of the bone tissue against deformation is higher (ie, greater elastic modulus), the strain of the collagen fibrils approaches the strain of the bone tissue. Interestingly, these changes are more pronounced in the diabetes cases shown by a twofold higher slope compared to the control cases. Therefore, samples from the diabetes groups with a lower elastic modulus also had a lower fibril-to-tissue strain ratio compared to control cases with similar elastic modulus. In combination with the observed tendency to higher CML accumulation (as observed in our previous study)[18] this may lead to the observed lower fibril deformation in T2DM and likely contribute to the increased fracture risk,[18,61] as shown by higher serum CML levels which were associated with increased risk of incident

clinical fractures in T2DM independent of BMD.[24] It is unclear what the mechanism is. Clearly, there is a complex relationship between mineralization, crosslinking and non-crosslinking AGEs, and collagen fibril deformation.

Limitations

The usage of a water phantom instead of human abdominal tissue to compensate for missing soft tissue as in in vivo DXA measurements and different scan regions, namely mid-diaphyseal femoral scan region, in HR-pQCT must be taken in account. Samples have been fixed for 7 seconds in 70% ethanol for synchrotron application and subsequently rehydrated prior to tensile testing, which might affect biomechanical properties. All samples have been treated the same way to allow for group comparison. This ex vivo study was performed on bone tissue which has been obtained during autopsy at the same skeletal region in all individuals assuring a generally longitudinal orientation of osteons. Due to the scarcity of human bone cores, the sample size is limited and comes along with age heterogeneity of the individuals. Although we were not able to determine the glycemic control, history of complications and diabetes duration due to the postmortem nature of the study, the advanced age of the studied cohort suggests late-stage DM with long-term treatments in both DM types, which might contribute to the small differences between both DM types. Information on DM treatment is limited to oral antidiabetics and insulin treatment, potential medication-related effects on the bone matrix might influence the herewith presented results and cannot be ruled out within this study. Nevertheless, it must be taken into account, that the glycemic control as well as diabetes-induced complications as well as the diabetes duration may affect bone quality. These effects cannot be fully discriminated within this study. The study was powered to detect differences in collagen fibril deformation; a larger sample size might identify additional significant differences in bone material quality parameters that remained undetected. Thus, influences of the limited sample size to the observed trends cannot fully be ruled out. By focusing on male individuals, a sex-related effect in terms of menopausal influences is avoided.

In conclusion, our study reveals that DM causes lower bone fibrillar deformation at the nanoscale and supports the hypothesis of a profound role of non-crosslinking AGEs in the pathophysiology of diabetic bone disease. Further studies analyzing CML, its detailed effect on bone protein and its correlation to fracture risk in DM patients are necessary to determine whether CML could serve as a potential clinical biomarker in diabetic fracture risk. To elucidate the underlying mechanism of fracture risk in T2DM further studies combining in-depth bone material quality analyses with a strong clinical characterization of the sample cohort are needed.

Acknowledgments

AUTHOR CONTRIBUTIONS

Eva Maria Wölfel: Conceptualization; funding acquisition; investigation; methodology; project administration; visualization; writing – original draft; writing – review and editing. **Felix Schmidt:** Investigation; methodology; writing – review and editing. **Annika vom Scheidt:** Methodology; writing – review and editing. **Anna Kornelia Siebels:** Methodology. **Birgit Wulff:** Methodology. **Herbert Mushumba:** Methodology. **Benjamin Ondruschka:** Methodology; resources; writing – review and editing. **Klaus Püschel:** Methodology. **Jean Scheijen:** Methodology. **Casper Schalkwijk:** Investigation; methodology; writing – review and editing. **Eik Vettorazzi:** Investigation; writing – review and editing. **Katharina Jähn-Rickert:** Funding acquisition; writing – review and editing. **Bernd Gludovatz:** Writing – review and editing. **Eric Schaible:** Investigation; methodology; writing – review and editing. **Michael Amling:** Methodology; project administration; resources. **Martina Rauner:** Funding acquisition; project administration; writing – review and editing. **Lorenz Hofbauer:** Funding acquisition; project administration; writing – review and editing. **Elizabeth A Zimmermann:** Conceptualization; funding acquisition; investigation; supervision; visualization; writing – original draft; writing – review and editing.

Conflict of Interest

All authors declare they have no conflicts of interest.

DATA AVAILABILITY STATEMENT

Data available on request due to privacy/ethical restrictions

References

1. Lin X, Xu Y, Pan X, et al. Global, regional, and national burden and trend of diabetes in 195 countries and territories: an analysis from 1990 to 2025. Sci Rep. 2020;10(5):14790.

2. Alzaid A, de Guevara PL, Beillat M, Lehner V, Atanasov P. Burden of disease and costs associated with type 2 diabetes in emerging and established markets: systematic review analyses. Expert Rev Pharmacoecon Outcomes Res. 2021;21(4):785-798.

3. Guntur AJ, Rosen CJ. NIH public access. Endocr Pract. 2012;18(5):758-762.

4. Napoli N, Strotmeyer ES, Ensrud KE, et al. Fracture risk in diabetic elderly men: the MrOS study. Diabetologia. 2014;57(10):2057-2065.

5. Janghorbani M, Feskanich D, Willett WC, Hu F. Prospective study of diabetes and risk of hip fracture: the nurses' health study. Diabetes Care. 2006;29(7):1573-1578.

6. Jiao H, Xiao E, Graves DT. Diabetes and its effect on bone and fracture healing. Curr Osteoporos Rep. 2015;13(5):327-335.

7. Martinez-Laguna D, Nogues X, Abrahamsen B, et al. Excess of all-cause mortality after a fracture in type 2 diabetic patients: a population-based cohort study. Osteoporos Int. 2017;28(9):2573-2581.

8. Starup-Linde J, Hygum K, Harsløf T, Langdahl B. Type 1 diabetes and bone fragility: links and risks. Diabetes Metab Syndr Obes. 2019;12:2539-2547.

9. Russo GT, Giandalia A, Romeo EL, et al. Fracture risk in type 2 diabetes: current perspectives and gender differences. Int J Endocrinol. 2016;2016:1615735.

10. Vestergaard P. Discrepancies in bone mineral density and fracture risk in patients with type 1 and type 2 diabetes - a meta-analysis. Osteoporos Int. 2007;18(4):427-444.

11. Moayeri A, Mohamadpour M, Mousavi SF, Shirzadpour E, Mohamadpour S, Amraei M. Fracture risk in patients with type 2 diabetes mellitus and possible risk factors: a systematic review and meta-analysis. Ther Clin Risk Manag. 2017;13:455-468.

12. Patsch JM, Burghardt AJ, Yap SP, et al. Increased cortical porosity in type 2 diabetic postmenopausal women with fragility fractures. J Bone Miner Res. 2013;28(2):313-324.

13. Shanbhogue VV, Hansen S, Frost M, et al. Bone geometry, volumetric density, microarchitecture, and estimated bone strength assessed by HR-pQCT in adult patients with type 1 diabetes mellitus. J Bone Miner Res. 2015;30(12):2188-2199.

14. Schwartz AV, Vittinghoff E, Bauer DC, et al. Association of BMD and FRAX score with risk of fracture in older adults with type 2 diabetes. JAMA. 2011;305(21):2184-2192.

15. Hofbauer LC, Busse B, Eastell R, et al. Bone fragility in diabetes: novel concepts and clinical implications. Lancet Diabetes Endocrinol. 2022;10(3):207-220.

16. Zimmermann EA, Schaible E, Bale H, et al. Age-related changes in the plasticity and toughness of human cortical bone at multiple length scales. Proc Natl Acad Sci U S A. 2011;108(35):14416-14421.

17. Gupta HS, Wagermaier W, Zickler GA, et al. Nanoscale deformation mechanisms in bone. Nano Lett. 2005;5(10):2108-2111.

18. Schwartz AV, Garnero P, Hillier TA, et al. Pentosidine and increased fracture risk in older adults with type 2 diabetes. J Clin Endocrinol Metabol. 2009;94(7):2380-2386.

19. Hunt HB, Torres AM, Palomino PM, et al. Altered tissue composition, microarchitecture, and mechanical performance in cancellous bone from men with type 2 diabetes mellitus. J Bone Miner Res. 2019;34(7):1191-1206.

20. Wölfel EM, Jähn-Rickert K, Schmidt FN, et al. Individuals with type 2 diabetes mellitus show dimorphic and heterogeneous patterns of loss in femoral bone quality. Bone. 2020;140(March):115556. https://doi.org/10.1016/j.bone.2020.115556.

21. Farlay D, Armas LAG, Gineyts E, Akhter MP, Recker RR, Boivin G. Nonenzymatic glycation and degree of mineralization are higher in bone from fractured patients with type 1 diabetes mellitus. J Bone Miner Res. 2016;31(1):190-195.

22. Karim L, Moulton J, van Vliet M, et al. Bone microarchitecture, biomechanical properties, and advanced glycation end-products in the proximal femur of adults with type 2 diabetes. Bone. 2018;114:32-39. https://doi.org/10.1016/j.bone.2018.05.030.

23. Thomas CJ, Cleland TP, Sroga GE, Vashishth D. Accumulation of carboxymethyl-lysine (CML) in human cortical bone. Bone. 2018;110:128-133.

24. Dhaliwal R, Ewing SK, Vashishth D, Semba RD, Schwartz AV. Greater carboxy-methyl-lysine is associated with increased fracture risk in type 2 diabetes. J Bone Miner Res. 2022;37(2):265-272.

25. Scheijen JLJM, Schalkwijk CG. Quantification of glyoxal, methylglyoxal and 3-deoxyglucosone in blood and plasma by ultra performance liquid chromatography tandem mass spectrometry: evaluation of blood specimen. Clin Chem Lab Med. 2014;52(1):85-91.

26. Tice MJL, Bailey S, Sroga GE, Gallagher EJ, Vashishth D. Non-obese mkr mouse model of type 2 diabetes reveals skeletal alterations in mineralization and material properties. JBMR Plus. 2022;6(2):e10583.

27. Holzer G, von Skrbensky G, Holzer LA, Pichl W. Hip fractures and the contribution of cortical versus trabecular bone to femoral neck strength. J Bone Miner Res. 2009;24(3):468-474.

28. Napoli N, Conte C, Eastell R, et al. Bone turnover markers do not predict fracture risk in type 2 diabetes. J Bone Miner Res. 2020;35(12):2363-2371.

29. Manavalan JS, Cremers S, Dempster DW, et al. Circulating osteogenic precursor cells in type 2 diabetes mellitus. J Clin Endocrinol Metabol. 2012;97(9):3240-3250.

30. Krakauer JC, McKenna MJ, Buderer NF, Sudhaker Rao D, Whitehouse FW, Parfitt MA. Bone loss and bone turnover in diabetes. Diabetes. 1995;44(7):775-782.

31. Vashishth D, Gibson GJ, Khoury JI, Schaffler MB, Kimura J, Fyhrie DP. Influence of nonenzymatic glycation on biomechanical properties of cortical bone. Bone. 2001;28(2):195-201.

32. Burghardt AJ, Issever AS, Schwartz AV, et al. High-resolution peripheral quantitative computed tomographic imaging of cortical and trabecular bone microarchitecture in patients with type 2 diabetes mellitus. J Clin Endocrinol Metabol. 2010;95(11):5045-5055.

33. Briggs AM, Wark JD, Kantor S, Fazzalari NL, Greig AM, Bennell KL. Bone mineral density distribution in thoracic and lumbar vertebrae: an ex vivo study using dual energy X-ray absorptiometry. Bone. 2006;38(2):286-288.

34. Burghardt AJ, Buie HR, Laib A, Majumdar S, Boyd SK. Reproducibility of direct quantitative measures of cortical bone microarchitecture of the distal radius and tibia by HR-pQCT. Bone. 2010;47(3):519-528.

35. Zimmermann EA, Schaible E, Gludovatz B, et al. Intrinsic mechanical behavior of femoral cortical bone in young, osteoporotic and bisphosphonate- treated individuals in low- and high energy fracture conditions. Sci Rep. 2016;6:21072. https://doi.org/10.1038/srep21072.

36. Granke M, Does MD, Nyman JS. The role of water compartments in the material properties of cortical bone. Calcif Tissue Int. 2015;97(3):292-307.

37. Lucksanasombool P, Higgs WAJ, Higgs RJED, Swain MV. Fracture toughness of bovine bone: influence of orientation and storage media. Biomaterials. 2001;22(23):3127-3132.

38. Hexemer A, Bras W, Glossinger J, et al. A SAXS/WAXS/GISAXS beamline with multilayer monochromator. J Phys Conf Ser. 2010;247:1-11.

39. Ilavsky J. Nika: software for two-dimensional data reduction. J Appl Crystallogr. 2012;45(2):324-328.

40. Roschger P, Fratzl P, Eschberger J, Klaushofer K. Validation of quantitative backscattered electron imaging for the measurement of mineral density distribution in human bone biopsies. Bone. 1998;23(4):319-326.

41. Milovanovic P, Zimmermann EA, Riedel C, et al. Multi-level characterization of human femoral cortices and their underlying osteocyte network reveal trends in quality of young, aged, osteoporotic and antiresorptive-treated bone. Biomaterials. 2015;45:46-55.

42. Schmidt FN, Zimmermann EA, Campbell GM, et al. Assessment of collagen quality associated with non-enzymatic cross-links in human bone using Fourier-transform infrared imaging. Bone. 2017;97:243-251. https://doi.org/10.1016/j.bone.2017.01.015.

43. Paschalis EP, Gamsjaeger S, Tatakis DN, Hassler N, Robins SP, Klaushofer K. Fourier transform infrared spectroscopic characterization of mineralizing type I collagen enzymatic trivalent cross-links. Calcif Tissue Int. 2014;96(1):18-29.

44. Paschalis EP, Mendelsohn R, Boskey AL. Infrared assessment of bone quality: a review. Clin Orthop Relat Res. 2011;469(8):2170-2178.

45. Arakawa S, Suzuki R, Kurosaka D, Ikeda R. Mass spectrometric quantitation of AGEs and enzymatic crosslinks in human cancellous bone. Sci Rep. 2020;10(18774):1-12.

46. Martens RJH, Broers NJH, Canaud B, et al. Relations of advanced glycation endproducts and dicarbonyls with endothelial dysfunction and low-grade inflammation in individuals with end-stage renal disease in the transition to renal replacement therapy: a cross- sectional observational study. PLoS One. 2019;14(8):e0221058.

47. Scheijen JLJM, van de Waarenburg MPH, Stehouwer CDA, Schalkwijk CG. Measurement of pentosidine in human plasma protein by a single-column high-performance liquid chromatography method with fluorescence detection. J Chromatogr B Analyt Technol Biomed Life Sci. 2009;877(7):610-614.

48. Viguet-Carrin S, Gineyts E, Bertholon C, Delmas PD. Simple and sensitive method for quantification of fluorescent enzymatic mature and senescent crosslinks of collagen in bone hydrolysate using single-column high performance liquid chromatography. J Chromatogr B Analyt Technol Biomed Life Sci. 2009;877(1-2):1-7.

49. Napoli N, Chandran M, Pierroz DD, Abrahamsen B, Schwartz AV, Ferrari SL. Mechanisms of diabetes mellitus-induced bone fragility. Nat Rev Endocrinol. 2017;13(4):208-219.

50. Janghorbani M, van Dam RM, Willett WC, Hu FB. Systematic review of type 1 and type 2 diabetes mellitus and risk of fracture. Am J Epidemiol. 2007;166(5):495-505.

51. Schwartz AV. Diabetes mellitus: does it affect bone? Calcif Tissue Int. 2003;73(6):515-519.

52. Gao H. Application of fracture mechanics concepts to hierarchical biomechanics of bone and bone-like materials. Int J Fract. 2006; 138(1-4):101-137.

53. Zimmermann EA, Riedel C, Schmidt FN, et al. Mechanical competence and bone quality develop during skeletal growth. J Bone Miner Res. 2019;34(8):1461-1472.

54. Gupta HS, Seto J, Wagermaier W, Zaslansky P, Boesecke P, Fratzl P. Cooperative deformation of mineral and collagen in bone at the nanoscale. Proc Natl Acad Sci U S A. 2006;103(47):17741-17746.

55. Acevedo C, Sylvia M, Schaible E, et al. Contributions of material properties and structure to increased bone fragility for a given bone mass in the UCD-T2DM rat model of type 2 diabetes. J Bone Miner Res. 2018;33(6):1066-1075.

56. Simmons ED, Pritzker KPH, Grynpas MD. Age-related changes in the human femoral cortex. J Orthoped Res. 1991;9(2):155-167.

57. Saito M, Marumo K. Collagen cross-links as a determinant of bone quality: a possible explanation for bone fragility in aging, osteoporosis, and diabetes mellitus. Osteoporos Int. 2010;21(2):195-214.

58. Saito M, Kida Y, Kato S, Marumo K. Diabetes, collagen, and bone quality. Curr Osteoporos Rep. 2014;12(2):181-188.

59. Nyman JS, Reyes M, Wang X. Effect of ultrastructural changes on the toughness of bone. Micron. 2005;36(7-8):566-582.

60. Sihota P, Yadav RN, Dhaliwal R, et al. Investigation of mechanical, material, and compositional determinants of human trabecular bone quality in type 2 diabetes. J Clin Endocrinol Metab. 2021;106(5): E2271-E2289.

61. Barzilay JI, Bůžková P, Zieman SJ, et al. Circulating levels of carboxy-methyl-lysine (CML) are associated with hip fracture risk: the cardiovascular health study. J Bone Miner Res. 2014;29(5):1061-1066.

62. Lamb LS, Alfonso H, Norman PE, et al. Advanced glycation end products and Esrage are associated with bone turnover and incidence of hip fracture in older men. J Clin Endocrinol Metab. 2018;103(11): 4224-4231.

63. Valderrábano RJ, Linares MI. Diabetes mellitus and bone health: epidemiology, etiology and implications for fracture risk stratification. Clin Diabetes Endocrinol. 2018;4(9):1-8.

64. Rey C, Combes C, Drouet C, et al. Surface properties of biomimetic nanocrystalline apatites: applications in biomaterials. Progress in Crystal Growth and Characterization of Materials. 2014;60(3-4):63-73.

65. Piccoli A, Cannata F, Strollo R, et al. Sclerostin regulation, microarchitecture, and advanced glycation end-products in the bone of elderly women with type 2 diabetes. J Bone Miner Res. 2020;35(12):2415-2422.